THE JOURNAL OF PHYSICAL CHEMISTRY B
A JOURNAL OF THE AMERICAN CHEMICAL SOCIETY

pubs.acs.org/JPCB

Article

Membrane Selectivity Mechanisms of the Antimicrobial Peptide Snakin-Z Against Prokaryotic and Eukaryotic Membrane Models

Nandan Kumar, Zhenjiao Du, Raghavendra G. Amachawadi, Xiaolong Guo, Jikai Zhao, and Yonghui Li*

Cite This: https://doi.org/10.1021/acs.jpcb.5c01013

Read Online

ACCESS | Metrics & More | Article Recommendations | Supporting Information

ABSTRACT: Snakin-Z, a novel cationic antimicrobial peptide (AMP) derived from *Zizyphus jujuba* fruits, exhibits broad-spectrum antimicrobial activity against bacteria and fungi. Importantly, it displays minimal hemolytic activity toward human red blood cells (RBCs). Elucidating the molecular basis of membrane selectivity of Snakin-Z is essential for its development as a novel antimicrobial agent. In this study, all-atom molecular dynamics (MD) simulations were employed to provide detailed molecular insights into the interactions between Snakin-Z and bacterial, fungal, and RBC membrane models. The simulations revealed a helical-coil conformation for Snakin-Z, with its amphipathic structure, polarity, and residues such as Arg, Lys, Ser, and Tyr playing crucial roles in mediating selective interactions with the microbial membrane models. Specifically, Arg28, Lys29, and Arg3 were identified as playing a crucial role in mediating membrane binding and stability. Snakin-Z was observed to be deeply embedded in the *Candida albicans* and *Bacillus subtilis* membrane models, followed by *Escherichia coli* and RBC membrane models. A considerable thinning and strong disordering of *Candida albicans*, *Bacillus subtilis* and *Escherichia coli* membranes acyl chains were observed. The presence of cholesterol in the RBC membrane contributes to its resistance to Snakin-Z-mediated disruption. This study presents the first comprehensive investigation of the selective mechanism underlying the antimicrobial activity of Snakin-Z against bacterial membrane models. Our findings provide insights into the antimicrobial properties of Snakin-Z at the molecular level, highlighting its significant potential for use in the food and biotechnology industries as a promising alternative to conventional antibiotics and preservatives.

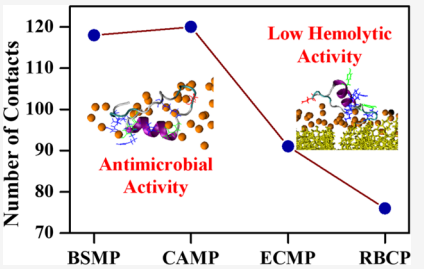

1. INTRODUCTION

The emergence of antibiotic-resistant pathogens poses a significant threat, not only to human health but also to global food security.[1−4] Food spoilage caused by microbial contamination leads to vast economic losses annually, with tons of usable food going to waste. Traditional methods for food preservation often rely on chemical preservatives, raising concerns about potential health risks and consumer preferences for natural solutions. This growing challenge underscores the urgent need for effective and safe alternatives.[5−11] Antimicrobial peptides (AMPs) have emerged as promising candidates due to their broad-spectrum activity against various foodborne pathogens.[12−14] AMPs are produced by all living organisms (bacteria, archaea, protozoa, fungi, plants, and animals) as part of their host defense mechanisms.[4] Plant-derived AMPs, in particular, offer a natural alternative for food preservation.[6,8−11] Snakin peptides have been identified as antipathogenic and have the potential to inhibit the growth of potato and wine grape pathogens.[15−18] One such Snakin with compelling potential is Snakin-Z, isolated from *Zizyphus jujuba*.[19] Snakin-Z exhibits remarkable antimicrobial activity at minimal concentrations (7.65−28.8 μg/mL) against a wide range of bacteria and fungi, including those responsible for food spoilage.[19] While previous studies have established its efficacy, the exact mechanism by which Snakin-Z disrupts microbial membranes remains unclear. Elucidating this mechanism is crucial for optimizing its use and for the rational design of even more potent AMPs.

In recent years, the activity of AMPs and their interactions with microbial membrane models have been investigated by using computational methods. These approaches have proven successful in providing valuable insights into the activity prediction and exploring the mechanisms of action for AMPs.[20−26,77,78] Computational modeling has enabled researchers to elucidate peptide−membrane interactions, including peptide binding mechanisms, as well as the structure and dynamics of membrane−peptide complexes.[20−26] Additional studies have further expanded our understanding of these interaction across different prototypical and membrane model systems.[27−31] In computational studies of AMPs, simulations often begin with a single peptide interacting with a membrane to elucidate fundamental interactions at the molecular level. This approach allows for a detailed understanding of the binding affinity of the peptide, the orientation, and the

Received: February 13, 2025
Revised: March 21, 2025
Accepted: April 16, 2025

Table 1. Considered Lipid Composition (%) of Prokaryotic Gram-Negative Bacteria Like *Escherichia coli* and Gram-Positive Bacteria Like *Bacillus subtilis*, Eukaryotic Red Blood Cells and Fungi Like *Candida albicans*

Simulation Systems		Acronym	Lipids (%)	# of Lipids	Box Size (nm^3)
Peptide in water	-	-	-	-	4.922 × 4.922 × 4.922
Pure membrane models	*Escherichia coli*	ECM	20POPG, 75POPE, 5CLP	256	9.089 × 9.089 × 16.500
	Bacillus subtilis	BSM	75POPG, 20POPE, 5CLP	256	9.349 × 9.349 × 16.500
	Candida albicans	CAM	3POPG, 26POPE, 25POPC, 18POPS, 20POPI, 7CLP, 1SSM	256	8.965 × 8.965 × 16.500
	Red blood cells	RBC	15POPE, 16POPC, 48CHL, 8SM, 13DOPS	256	8.206 × 8.206 × 16.500
Membrane-peptides models	*Escherichia coli*	ECMP	20POPG, 75POPE, 5CLP	256	9.279 × 9.279 × 14.853
	Bacillus subtilis	BSMP	70POPG, 20POPE, 5CLP	256	9.433 × 9.433 × 14.403
	Candida albicans	CAMP	3POPG, 26POPE, 25POPC, 18POPS, 20POPI, 7CLP, 1SSM	256	8.963 × 8.963 × 15.563
	Red blood cells	RBCP	15POPE, 16POPC, 48CHL, 8SM, 13DOPS	256	7.294 × 7.29 × 19.151

insertion dynamics within the lipid bilayer. For instance, simulations have been instrumental in determining the functionality of membrane-active AMPs, providing insights into their mechanisms of action. However, recognizing that AMP mechanisms are often cooperative, such as through pore formation involving multiple peptides, it is essential to extend these studies to include simulations with multiple peptides and varying concentrations.[20,21,24−26] This study employs computational modeling approaches for the first time to investigate the binding mechanism of Snakin-Z with bacteria, fungi, and red blood cell (RBC) membrane models. First, we utilized *ab initio* modeling and MD simulations followed by free energy landscape (FEL) analysis to predict the Snakin-Z structure. Then, we elucidated how Snakin-Z recognizes and interacts with these membrane models. This novel approach allows us to explore the intricate molecular details of these interactions, providing valuable insights into the selectivity of Snakin-Z toward its targets. Specifically, we constructed detailed membrane models using a range of lipids including phosphatidylglycerol (POPG), phosphatidylethanolamine (POPE), phosphatidylcholine (POPC), phosphatidylserine (POPS), phosphatidylinositol (POPI), cardiolipin (CLP), cholesterol (CHL), sphingomyelin (SM), and dioleoylphosphatidylserine (DOPS). These lipids represent the diverse compositions of prokaryotic Gram-negative bacteria like *Escherichia coli*,[32] and Gram-positive bacteria like *Bacillus subtilis*,[33] eukaryotic RBCs,[34,81,82] and fungi like *Candida albicans*,[35,81] as summarized in Table 1. The lipid composition of the *Candida albicans* model membrane includes POPC, POPE, POPI, POPS, and trace amounts of CLP, based on studies reporting its presence under specific conditions, though its abundance may vary by strain or experimental context.[81] This composition reflects the dynamic nature of fungal lipid profiles and provides a biologically relevant framework for studying peptide−membrane interactions.[81,85−87] The simulations were conducted using a symmetric membrane model with identical lipid compositions in both leaflets of the bilayer. While erythrocyte membranes typically exclude phosphatidylserine (PS) from the outer monolayer under normal physiological conditions, we included DOPS due to its well-documented relevance in membrane interactions and dynamics.[82,83] DOPS has been shown to play a significant role in membrane properties, particularly under conditions such as membrane activation or remodeling. We acknowledge that 1-palmitoyl-2-oleoyl-*sn*-glycero-3-phosphocholine (POPC), 1-palmitoyl-2-linoleoyl-*sn*-glycero-3-phosphocholine (PLPC), and 1-stearoyl-2-linoleoyl-*sn*-glycero-3-phosphocholine (SLPC) predominant in the outer leaflet of erythrocyte membranes.[84] Future studies will explore asymmetric membrane models to better mimic biological conditions. This study is limited to using simplified model membranes, which lack the full chemical complexity of natural biological membranes. Additionally, factors such as membrane curvature and membrane protein dynamics, which could influence peptide interactions, were not considered. These limitations should be acknowledged when our findings are applied to more complex biological systems. By elucidating the binding mechanism of Snakin-Z at the atomic level, this research offers valuable insights for developing next-generation antimicrobials derived from plants. These findings can guide the design of more targeted and potent AMPs with minimal impact on human health, offering safer and more effective strategies to combat food spoilage caused by microbial pathogens.

2. COMPUTATIONAL METHODS

2.1. Sequence Retrieval and Structural Modeling of the Snakin-Z Peptide. The Snakin-Z peptide sequence "CARLNCVPKGTSGNTETCPCYASLHSCRKYG" was retrieved from the Antimicrobial Peptide Database (APD ID: AP02258).[36] The structure of the peptide was modeled using the I-TASSER server, a hierarchical tool for predicting the protein structure. I-TASSER automatically identifies templates from the Protein Data Bank (PDB) through a multi-threading approach.[37] Full-length models are constructed by using iterative template-based and fragment-based simulations. The best model was selected based on C-score, TM-score, and root-mean-square deviation (RMSD), which indicate the quality and reliability of the predicted structure. The predicted structure was then subjected to three independent, one-microsecond (1 μs) MD simulations to investigate the conformational dynamics of the peptide. The FEL was analyzed to visualize the conformational preferences of the peptide, revealing regions of stability and flexibility. This analysis provided insights into the energetically favorable conformations adopted by the peptide. The structure with the lowest local energy from one of the replicas was selected for further study with the microbial membrane models. The secondary structure of the peptide was assigned using STRIDE,[79] a widely used algorithm for secondary structure determination from atomic coordinates. STRIDE combines hydrogen bond energy calculations and backbone dihedral angle analysis to classify protein structures into secondary structure elements, including alpha-helices, 3_{10}-helices, beta-strands, turns, and coils. Alpha-helices are identified by

https://doi.org/10.1021/acs.jpcb.5c01013
J. Phys. Chem. B XXXX, XXX, XXX−XXX

characteristic dihedral angles ($\varphi \approx -60°$, $\psi \approx -45°$) and hydrogen bonds between the carbonyl oxygen of residue i and the amide hydrogen of residue i + 4, while 3_{10}-helices are characterized by tighter helical turns and hydrogen bonds between residues i and i + 3. Turns are defined by specific hydrogen bonding patterns and dihedral angles, including beta-turns (e.g., Turn II and Turn IV) and gamma-turns, and coils represent regions lacking regular secondary structure patterns. STRIDE was applied to both the I-TASSER-predicted model and the global minima structure from the MD simulation for secondary structure assignments.

2.2. Construction of the Membrane Models. The initial lipid bilayer structures were generated for *Bacillus subtilis*, *Candida albicans*, *Escherichia coli*, and RBC using the CHARMM-GUI web server.[38] These models were constructed with the specific lipid compositions characteristic of each membrane type, as detailed in Table 1. To ensure the membrane models behaved realistically, they were first simulated for 1 μs in their "pure" state, without the Snakin-Z peptide present. This equilibration process allowed the membrane models to settle into a stable configuration. The final snapshots of these equilibrated pure membrane models were then used as the starting points for simulations involving the Snakin-Z peptide. The Snakin-Z structure was positioned approximately 6 nm away from the membrane surface, measured between the centers of mass (COM) of the peptide and the membrane models. We acknowledge that using the I-TASSER-predicted helical conformation (refinedby MD) may introduce a bias. This initial conformation was chosen to reflect the helical tendencies observed in the antimicrobial peptide. Finally, these membrane−peptide systems were subjected to three independent 1 μs MD simulations to elucidate the initial interaction and early stages of Snakin-Z peptide insertion into the membranes. This simulation length is sufficient for studying peptide−membrane interactions and the early insertion of the peptide into the bilayer models.[39−41]

2.3. Simulation Protocols. All MD simulations were performed with the GROMACS package, version 2023.3.[42] The CHARMM36m force field was used for all bilayer membrane models, while CHARMM36-jul2022 was used for the peptide.[43,44] All simulations were conducted with a salt concentration of 0.15 M NaCl, consistent with the physiological conditions. Sodium (Na^+) and chloride (Cl^-) ions were added to neutralize the system's charge and achieve the specified salt concentration. A 2.5 nm layer of water was added on each side of the membrane, resulting in a total water layer thickness of 5 nm in the z-direction. Table 1 summarizes the lipid composition and simulation box sizes for the different membrane systems considered in this study. The periodic boundary conditions (PBC) were applied in all simulation box axes, and the TIP3P water model[45] was used to solvate the systems. The protocol defined by CHARMM-GUI was adopted to prepare the simulation system,[38,46] which includes steepest descent energy minimization to eliminate any high-energy configurations, guaranteeing a stable starting point for the simulation. The system underwent a series of six equilibration steps, during which restraints on the lipids were gradually reduced (starting from 1000 kJ/mol).[47] This process allowed the lipids to relax and adopt their natural conformations. The system was then equilibrated at a constant volume (NVT) in two stages: first with constraints applied, followed by a relaxed simulation without constraints. Finally, constant pressure and temperature (NPT) equilibration was performed, also involving constrained and relaxed phases. Finally, 1 μs production MD simulations were conducted for both the pure membrane models and the membrane−peptide complexes. Trajectories were saved every 2 ps for further analysis. The Nosé-Hoover thermostat was used to maintain a constant temperature of 310.15 K with a coupling constant of 0.2 ps. A semi-isotropic Parrinello−Rahman barostat ensured a constant pressure of 1 atm with a compressibility of 4.5×10^{-5}/bar and a coupling constant of 1 ps.[48−50] The LINCS algorithm was used to constrain hydrogen bonds,[51] and the Particle Mesh Ewald (PME) method[52,53] was used to efficiently calculate long-range electrostatic interactions with a short-range cutoff of 12 Å. A switching function starting at 10 Å ensured a smooth transition for van der Waals interactions to zero at a 12 Å cutoff distance.

2.4. Analysis. The MD trajectories were analyzed using GROMACS utilities, VMD,[54] and MDAnalysis.[55] Principal component analysis (PCA) was performed based on the diagonalization of the covariance matrix of the peptide trajectory, and the FELs were projected onto the first two principal components. The helical wheel projection of the peptide was performed using the online tool (https://www.donarmstrong.com/cgi-bin/wheel.pl). Area per lipid (APL) and membrane thickness were calculated using MEMPLUGIN of VMD and MDAnalysis.[56,80] The membrane thickness was calculated by selecting the phosphate atoms (name P) of the lipid headgroups and computing the average distance between the upper and lower leaflets along the Z-axis for each frame of the trajectory. Similarly, APL was calculated by selecting the phosphate atoms (name P) of the lipid headgroups and computing the area of the simulation box in the XY-plane divided by the number of lipids in the upper leaflet for each frame of the trajectory. The helicity of the peptide was calculated using the "gmx helix" tools. The Radial Distribution Function (RDF), $g(r)$, measures the probability of finding a particle at a distance r from a reference particle, normalized by the bulk density. It is computed using "gmx rdf" by calculating pairwise distances between reference and target groups, binning them into intervals, and normalizing by the volume of spherical shells and bulk density. Deuterium order parameters (S_{CH}) for the acyl chains were calculated by analyzing the orientational mobility of the C−H bonds along the chains. As shown in eq 1, S_{CH} is determined by the average angle (θ) between the C−H bond vector and the normal to the membrane. This calculation reflects the time-averaged motional freedom of the acyl chains.

$$S_{CH} = \left| \left\langle \frac{3\cos^2\theta - 1}{2} \right\rangle \right| \tag{1}$$

To examine the extent of exposure between the membrane and the peptides, we calculated the contact area between the peptide and each membrane. This contact area was derived by using solvent-accessible surface area (SASA) calculations. The contact area at a given time t, denoted as $A(t)$, was determined using the eq 2.

$$A(t) = \frac{a_{membrane}(t) + a_{peptide}(t) - a_{membrane-peptide}(t)}{2} \tag{2}$$

where, $a_{membrane}(t)$ is the SASA of the membrane alone at time t, $a_{peptide}(t)$ is the SASA of the peptide alone at time t, and $a_{membrane-peptide}(t)$ is the SASA of the combined membrane−

https://doi.org/10.1021/acs.jpcb.5c01013
J. Phys. Chem. B XXXX, XXX, XXX−XXX

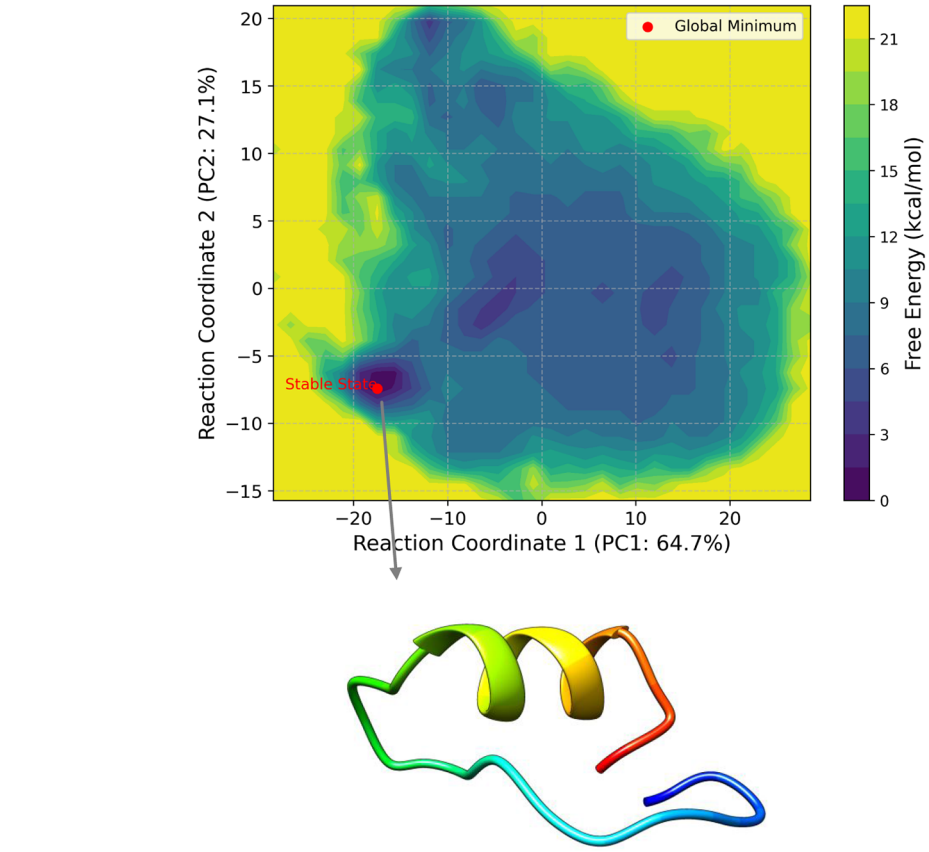

(A)

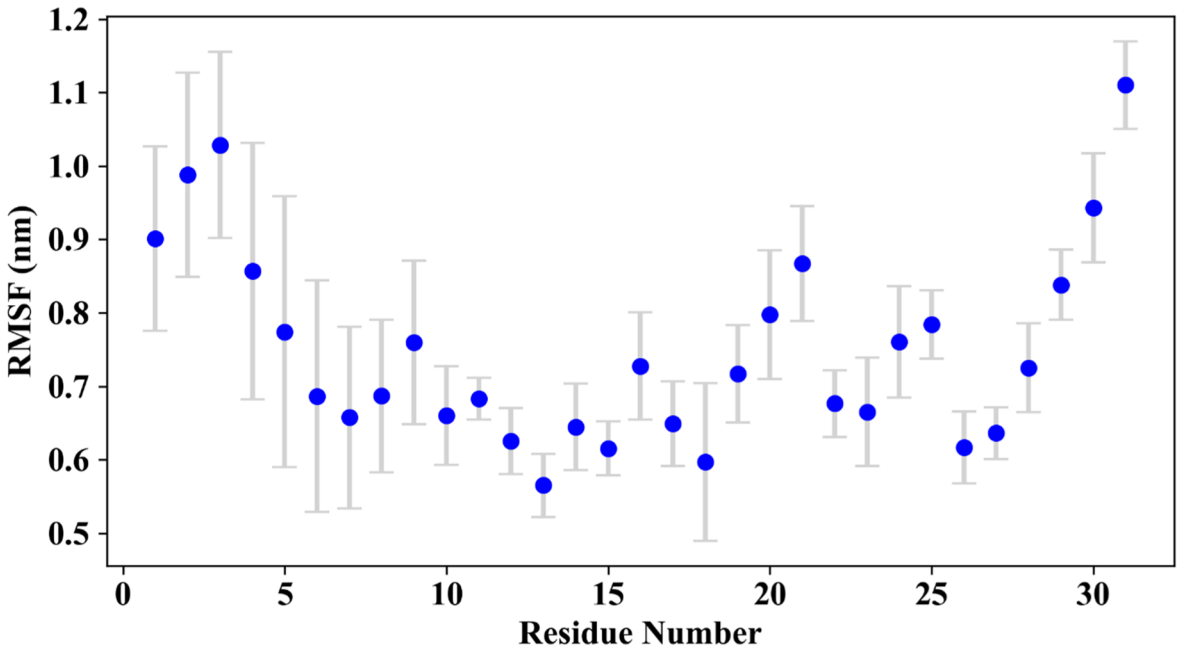

(B)

Figure 1. (A) 2D Free energy landscape (FEL) of Snakin-Z conformations along the first two principal components (PC1 and PC2). The color gradient represents free energy (kcal/mol), with darker regions indicating lower-energy, more stable conformations, and lighter regions representing higher-energy states. The global minimum, corresponding to the most stable conformation, is marked with a red dot and labeled as the stable state. The corresponding structure of this stable conformation is shown below the 2D FEL plot. (B) The root-mean-square fluctuation (RMSF) values of peptide residues with error bars representing mean ± standard deviation. Error bars indicate the variability of RMSF for each residue.

https://doi.org/10.1021/acs.jpcb.5c01013
J. Phys. Chem. B XXXX, XXX, XXX−XXX

peptide system at time t. The SASA values were calculated by using the GROMACS gmx sasa tool, which estimates the surface area accessible to a solvent by rolling a virtual probe of a specified radius (1.4 Å in this case, mimicking the radius of a water molecule) over the surface of the molecule.

2.5. Statistical Analysis. All quantitative metrics were calculated from triplicate MD simulations. Data are presented as mean ± standard error of the mean (SEM), where SEM was calculated as the standard deviation divided by the square root of the number of replicates ($n = 3$). Statistical significance was assessed using one-way ANOVA followed by Tukey's HSD posthoc test for multiple comparisons. Differences were considered statistically significant at $p < 0.05$. Statistical analysis was performed using Python (SciPy and statsmodels libraries).

3. RESULTS AND DISCUSSION

3.1. Structural Modeling and Dynamics of the Snakin-Z Peptide. The I-TASSER modeling was employed to generate a structural model of Snakin-Z. The reliability of the model was assessed based on a combination of favorable metrics indicative of good quality: C-score (−0.56), normalized C-score (−0.56), cluster density (0.3765), Exp.TM-Score (0.64), and Exp.RMSD (2.80). These metrics are crucial, with the C-score reflecting the confidence in the model, and the cluster density, Exp.TM-Score, and Exp.RMSD providing insight into the model's structural accuracy and similarity to native structures. Notably, the initial predicted conformation obtained from I-TASSER displayed a mainly helical structure (Figure S1A), which is in accordance with the secondary structure reported for the recombinant Snakin-Z and other Snakin peptides.[17,57,58] The predicted structure also aligns with observations for other antimicrobial peptides, known for their helical conformations that facilitate interaction with microbial membranes.[12,57,59] However, we acknowledge that structural variations exist among Snakin family members, with some predicted models also exhibiting β-strands.

To minimize the potential bias in the modeled Snakin-Z structure and to further explore its conformational preferences and stability, we performed three independent 1-μs MD simulations to comprehensively capture its dynamic behavior. PCA was then performed on the diagonalization of the covariance matrix derived from these simulations, allowing a low-dimensional representation of conformational motion. Specifically, the first two principal components (PC1 and PC2), which capture the largest variance, were used as reaction coordinates to construct the Free Energy Landscape (FEL), as shown in Figure 1A. The 2D FEL of Snakin-Z revealed a prominent global minimum located at approximately (−17, −7), corresponding to the most thermodynamically stable conformation under physiological conditions. Surrounding this region, gradually increasing free energy contours indicate fewer stable conformations that the peptide can adopt. These alternative states, while higher in energy, suggest structural flexibility that may be crucial for biological interactions. The higher-energy plateau (up to ∼21 kcal/mol) represents transient, unfolded-like conformations that are rarely populated but highlight the conformational adaptability of the peptide.

The secondary structure of the peptide was analyzed using STRIDE.[79] The initial structure, predicted using I-TASSER, displayed a predominantly helical conformation, with an α-helix spanning residues 19−27 and a 3_{10}-helix spanning residues 15−17, along with several turns and coils (Table 2). To validate the stability of this conformation, we performed 1-μs MD simulations. The global minimum structure from the MD simulation retained a stable α-helix spanning residues 20−28, consistent with the initial prediction, while other regions adopted coil or turn conformations. This confirms the stability of the helical segment and provides insights into the structural behavior of the Snakin-Z model in a dynamic environment. The helical conformation of Snakin-Z is consistent with observations for other AMPs, which adopt amphipathic α-helical structures upon interaction with lipid membranes. This structural transition is associated with the amphipathic nature of AMPs, allowing them to interact with both the hydrophobic core and the hydrophilic headgroups of the membrane. Helical wheel analysis of Snakin-Z reveals charged residues segregated to one face of the helix and hydrophobic residues to the other, enhancing its interactions with lipid bilayers. This amphipathic arrangement is similar to that observed in other AMPs, such as melittin, which forms a bent, rod-like conformation with two α-helical parts when bound to lipid membranes. The higher hydrophobicity and hydrophobic moment of Snakin-Z, compared to peptides like Plantaricin CS, correlate with its increased membrane interactions and hemolytic activity, a common feature among AMPs that influences their ability to disrupt membrane integrity.[91,92]

Table 2. Secondary Structure Details of Snakin-Z[a]

Residue Range	I-TASSER Model	Residue Range	MD Simulation (Global Minima)
1−5	Turn	1−11	Coil
6−7	Coil	12−15	Turn
8−14	Turn	16−19	Coil
15−17	3_{10}-Helix	20−28	Alpha-helix
18	Coil	28−31	Coil
19−27	Alpha-helix		
28−30	Turn		
31	Coil		

[a]The table compares the secondary structure assignments from the I-TASSER model and the MD simulation (global minima) for different residue ranges, highlighting the presence of turns, coils, and helices in both models.

The helical wheel plot of the peptide demonstrates a clear amphipathic nature with distinct hydrophobic and hydrophilic faces, as shown in Figure S1B. The hydrophilic residues 11T, 12S, 15T, 17T, and 23S cluster on one side, indicating potential interactions with aqueous environments or other polar molecules. Conversely, hydrophobic residues 1C, 18C, 27C, 30Y, 4L, 2A, 24L, and 22A form a hydrophobic face, suggesting interactions with lipid membranes or other hydrophobic surfaces. Additionally, potentially charged residues such as 16E, 9K, 3R, 28R, and 29K indicate areas that might engage in strong electrostatic interactions with anionic lipids. The amphipathic property of the peptide and its helical structure are typical characteristics of peptides involved in membrane interactions. Further root-mean-square fluctuation (RMSF) of the peptide residues across the three replicas was computed. The means and SD of RMSF values for each residue were computed and are presented in Figure 1B, suggesting variability between the replicas for a few of the residues. Although there is variability across the replicas, the error bars (representing ± 1 SD) show that many of the

https://doi.org/10.1021/acs.jpcb.5c01013
J. Phys. Chem. B XXXX, XXX, XXX−XXX

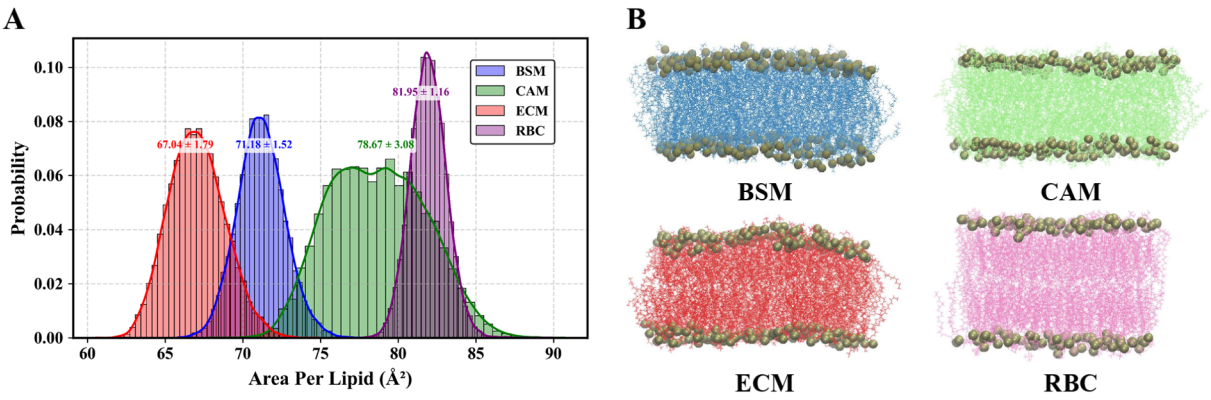

Figure 2. Equilibration of membrane systems through area per lipid (APL) distribution. (A) Probability density plots of the area per lipid (APL) distribution for the BSM, CAM, ECM, and RBC membrane models. (B) Representative structures of the equilibrated membrane models, demonstrating their structural integrity and stability.

residues exhibit overlapping error bars, suggesting limited statistical significance in the differences for individual residues between replicas. The residues with the largest RMSF (indicating the highest flexibility) are found at the N- and C-terminal regions of the peptide. The residues from 9K to 27C have lower RMSF, suggesting relative rigidity compared to other regions. Specifically, residues 20C to 27C of the helical region were observed to have the lowest RMSF (Figure 1B). This signifies that regions near the deep energy well correspond to stable segments of the peptide, associated with helical structures critical for maintaining the peptide's bioactive conformation. Conversely, regions further from the energy well, representing flexible loops or terminal regions, exhibit higher RMSF values, potentially facilitating adaptation to various binding partners.

3.2. Behavior of the Peptide Toward the Membrane.

3.2.1. Structural Changes of Membrane–Peptide Complexes. We first assessed the equilibration of the membrane systems by analyzing the area per lipid (APL) distribution, a critical parameter that reflects the lipid packing density and membrane stability. The probability density plots (Figure 2A) reveal that each membrane model—BSM, CAM, ECM, and RBC—exhibits a distinct yet well-defined APL distribution, indicating convergence to an equilibrium state. The absence of significant drifts or broad multimodal distributions in the APL profiles further supports the conclusion that the systems were fully equilibrated. Additionally, representative structures of the equilibrated membrane models are shown in Figure 2B, providing a visual confirmation of their structural integrity and stability. The lowest energy conformation of Snakin-Z was used to investigate its selectivity toward these equilibrated BSM, CAM, ECM, and RBC membrane models through three independent 1microsecond MD simulations for each membrane system. Cluster analysis, a computational technique used to discern patterns in MD simulations, was employed with an RMSD cutoff of 3.5 nm to inspect the binding behaviors of peptide–membrane complexes. The results elucidated distinct structural dynamics among these membrane models, as shown in Table S1 and Figure S2. Notably, CAMP exhibited a rich diversity of conformations, evidenced by the highest number of clusters (ranging from 44 to 48). The distribution of frames among the top clusters is uniform, with each of the top five clusters capturing between 5.06% and 7.50% of the frames. This uniform distribution indicates that the CAMP experiences substantial structural/conformational changes during its interaction with Snakin-Z peptide.

In addition to CAMP, BSMP and ECMP also demonstrated reasonable structural variability, as indicated by 19–24 and 21–22 clusters, respectively. The percentage of frames assigned to the top five clusters indicates moderate clustering variability across simulations. Conversely, RBCP exhibited the least structural diversity, with only 3–6 clusters, implying minimal conformational changes thzroughout the simulation, as shown in Table S1. These findings provide insights into the differential responses of membrane models to Snakin-Z peptide interaction. The abundance of clusters in CAMP suggests a dynamic interaction, potentially leading to significant membrane perturbation. In contrast, the limited cluster distribution in RBCP indicates a static or rigid membrane environment, with negligible perturbation induced by Snakin-Z. Specifically, the RBCP shows a dominant single cluster that accounts for the majority of frames (89.66% on average), while the remaining clusters contribute minimally (Table S1), signifying a lack of structural variability, suggesting that Snakin-Z may exert minimal influence on the ordering of the RBC membrane model. Figure S2 presents the representative structures of each cluster from one of the replicas, highlighting the dominant conformational states of both the membranes and the peptides in each complex. The peptide conformations reflect their structural adaptation to different lipid environments. In CAMP, where multiple clusters have a uniform distribution, peptides exhibit diverse conformations, suggesting flexibility in interacting with the complex membrane composition. In contrast, the RBCP, dominated by a single cluster, shows a membrane–peptide complex in a highly stable conformation, indicating limited structural variability. These results illustrate the interplay between peptides and lipid environments, influencing the conformational behavior of the membrane–peptide complexes. The conformational diversity observed in some AMPs is reminiscent of the behavior of temporins, which exhibit distinct interaction modes depending on membrane composition. For example, temporin B displays considerable conformational flexibility, particularly from the N- to C-terminus, when interacting with both POPE/POPG and POPG membranes.[93] In contrast, other AMPs, such as LL-37, show more limited conformational changes in specific membrane environments. LL-37 remains parallel to the membrane surface throughout its action and does not insert

https://doi.org/10.1021/acs.jpcb.5c01013
J. Phys. Chem. B XXXX, XXX, XXX–XXX

deeply into the bilayer, with its orientation largely unaffected by factors such as membrane charge or ionic conditions.[94,95] These examples highlight the diverse mechanisms by which AMPs adapt to different membrane environments, underscoring the importance of lipid composition in modulating peptide−membrane interactions.

Figure 3 depicts the representative structure and orientation of a peptide in its unbound and bound states. Table S1

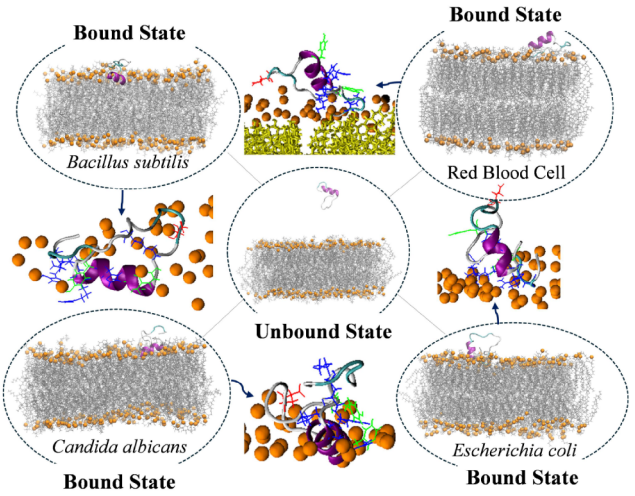

Figure 3. Representative structure and orientation of the peptide in unbound and bound states. The peptide structure is depicted as a cartoon model, while lipid acyl chains are represented by lines and colored gray. The P atoms are depicted as spheres and are colored orange. Aromatic, basic, and acidic residues are also represented by lines and are colored green, blue, and red, respectively. Cholesterol is shown in yellow in color in the case of red blood cells.

provides the total number of clusters obtained from the cluster analysis, along with the percentage of frames found in the top five clusters. Figure S2 illustrates the representative structures of the peptide in its bound state with the membrane model corresponding to the top five clusters. These clusters reveal a fascinating interplay between the orientation of the peptide and the specific lipid composition of the membrane. For membrane models enriched with negatively charged POPG, i.e., BSMP and CAMP, a preferential interaction is suggested. The positively charged residues at the N-terminus of the peptide might be electrostatically attracted to the negatively charged POPG headgroups. This interaction acts as an anchor, allowing the hydrophobic helical region to insert itself favorably into the core of the membrane model (Figure 3). In contrast, for membrane models with a lower POPG content (RBCP and ECMP), a less defined interaction pattern is indicated. The peptide might transiently interact with the membrane surface through both N- and C-terminal regions, potentially reflecting a search for a favorable binding site due to the reduced electrostatic anchoring from POPG. Interestingly, the presence of cholesterol in RBCP compared to ECMP might further influence peptide penetration (Figures 3 and S3). Cholesterol, with its rigid structure, could act as a barrier, potentially hindering the ability of the peptide to insert into the membrane.[34,41]

3.2.2. Proximity of the Peptide to the Membrane. To assess the proximity of the peptide to the bilayer models, the z-coordinates of the center of mass (COM) of the peptide and the COM of the membrane were calculated as a function of time (Figure 4A). The results indicate that the peptide rapidly approaches the membrane surface, typically within the first 50−100 ns, in all three independent simulations, suggesting that the peptide has a strong initial affinity for the membrane interface, as shown in Figure 4A. Depending on the nature and composition of the membrane models, primarily the C- and N-terminal residues were observed to approach the membrane in close proximity, while the central region of the peptide remained unable to adsorb onto the membrane surface, as evidenced by the distance between the residues and the peptide (Figure S3). This could be due to its polar and hydrophilic nature, which favors aqueous environments over the hydrophobic core of the membrane. Following the analysis of the perpendicular distance of the peptide from the membrane (Figure 4A), representative structural snapshots at different time points (0, 100, 500, and 1000 ns) provide a visual depiction of the dynamic interactions of the peptide with the membrane models (Figure 4B). These snapshots illustrate the initial approach, membrane attachment, and subsequent conformational changes over time, highlighting key transitions such as the orientation and depth of embedding of the peptide on the membrane model surface.

Figure 5A illustrates the average distance between the peptide and the membrane surface across different membrane models (BSMP, CAMP, ECMP, and RBCP). The average distances for the BSMP and CAMP membrane models were close, measuring 2.6 ± 0.2 nm and 2.7 ± 0.1 nm, respectively. The peptide exhibited a larger average distance from the ECMP and RBCP membrane models, with values of 3.0 ± 0.4 nm and 3.3 ± 0.2 nm, respectively. Statistical analysis revealed that the distance for RBCP was significantly larger than for BSMP (p = 0.013), CAMP (p = 0.010), and ECMP (p = 0.007). No significant differences were observed between BSMP, CAMP, and ECMP (all $p > 0.05$). These observations suggest stronger interactions between the peptide and the BSMP and CAMP membrane models, compared to the weaker interactions observed with ECMP and RBCP membrane models. For both BSMP and CAMP, the C- and N- terminal regions (residues 2A to 6C and 19P to 30Y, respectively) appeared to embed themselves on the membrane surface. Notably, residues such as 3R, 4L, 28R, and 29K, along with a few other cationic and aromatic residues, seemed to penetrate the surface of the membrane models, as the measured distance between the center of mass (COM) of these residues and the phosphorus atoms of the membrane was ≤ 2.0 nm. Similarly, these residues were near the membrane surface for ECMP, though the distances slightly exceeded 2.0 nm. This close association can be attributed to the higher content of negatively charged POPG in CAMP and BSMP membrane models, followed by ECMP. The negatively charged headgroup of POPG facilitates strong electrostatic interactions with the positively charged residues in Snakin-Z, promoting penetration. In contrast, the peptide exhibited weaker interactions with RBCP membrane models, where most residues remained approximately 3.0 nm away from the membrane surface, with only a few residues making closer contact (Figure S3). This observation can be explained by the lower content of POPG in these membranes, as well as in RBCP, which also contains CHL, and its bulky structure and neutral charge can hinder close peptide−membrane contact and reduce the electrostatic attraction between the peptide and the membrane. These findings highlight the crucial role of anionic lipids, particularly POPG, in mediating Snakin-Z binding affinity. However, other

https://doi.org/10.1021/acs.jpcb.5c01013
J. Phys. Chem. B XXXX, XXX, XXX−XXX

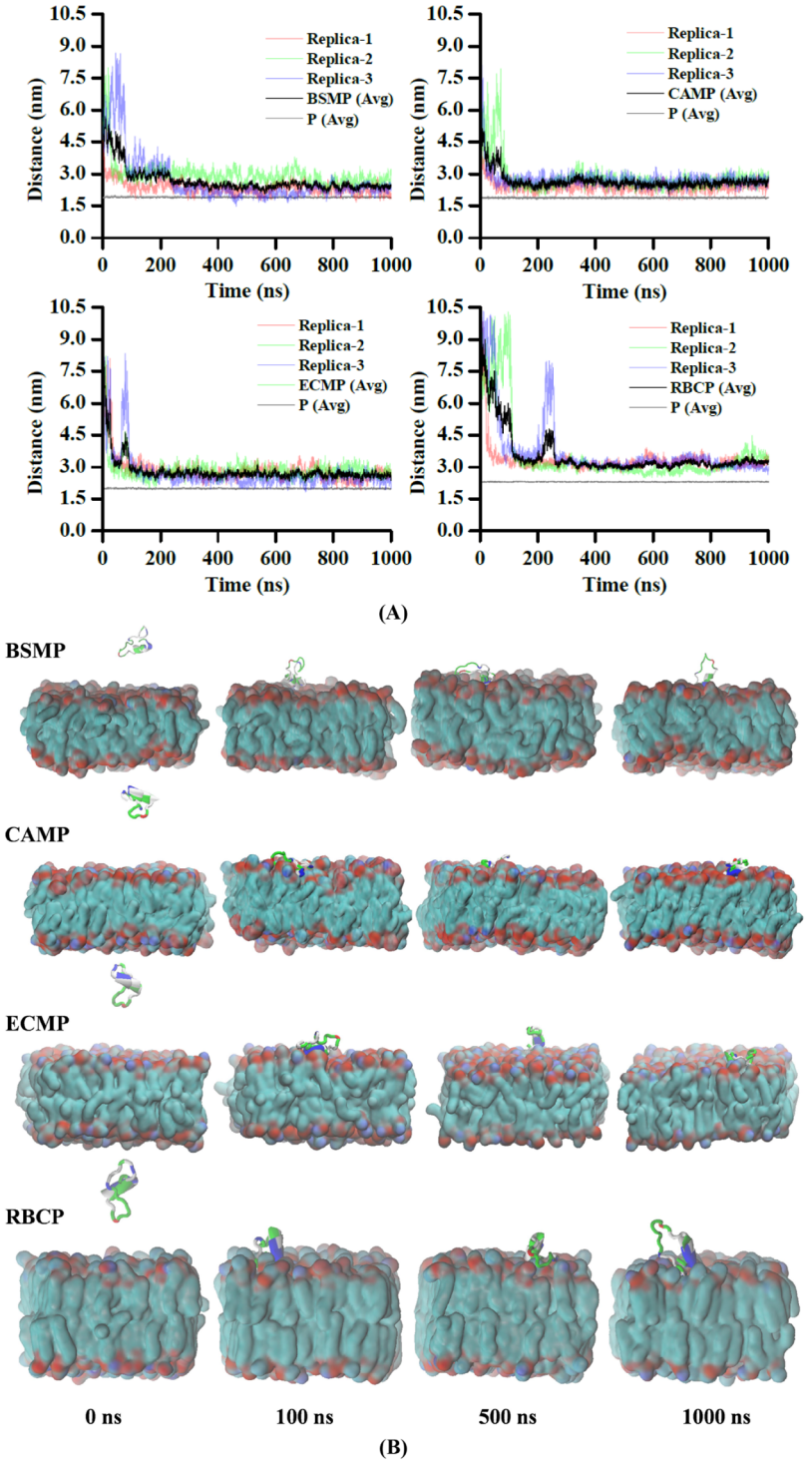

Figure 4. (A) Perpendicular distance between the center of mass (COM) of the peptide and the membrane throughout the simulation. The average distance of the three replica is shown in black in color. (B) Representative snapshots of the peptide−membrane system at different time points during the simulation (0, 100, 500, and 1000 ns), visualized using VMD. The peptide is shown in cartoon representation and colored based on residue type, while the membrane models are depicted using the quick surface representation and colored by atom name. These snapshots illustrate the dynamic changes in the position of the peptide relative to the membrane over time.

negatively charged lipids like POPS present in CAMP might also contribute to the strong interaction observed. Additionally, the presence of neutral lipids like POPE and POPC in all membrane models influences peptide−membrane interactions by creating a more flexible and fluid environment compared to membranes solely composed of rigid, cholesterol-rich structures like RBCP.

Previous studies have demonstrated that increasing the CHL content in anionic lipid bilayers can hinder the ability of antimicrobial peptides to penetrate the hydrophobic core. The rigid structure of CHL is believed to create a more tightly packed membrane, effectively excluding peptides from deeper insertion. Additionally, cholesterol may help maintain membrane integrity during interactions with proteins or pep-

https://doi.org/10.1021/acs.jpcb.5c01013
J. Phys. Chem. B XXXX, XXX, XXX−XXX

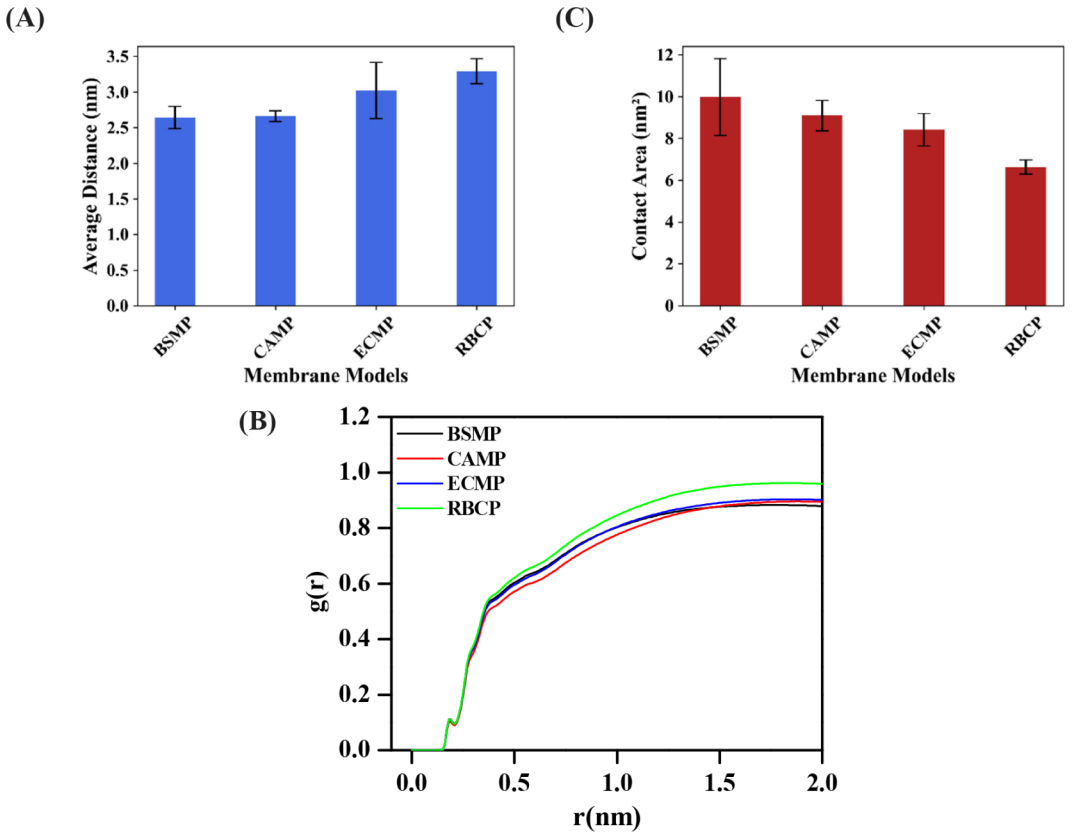

Figure 5. (A) Average distance between the peptide and the P atom of the membrane. (B) Radial distribution function (RDF) of water molecules around peptides in BSMP, CAMP, ECMP, and RBCP membrane complexes. (C) Contact areas between membrane and peptide. Error bars represent the standard error of the mean from triplicate measurements.

tides.[34,41,60] In accordance with these findings, our simulations with RBCP, which has a high cholesterol content, revealed limited close-range interaction between Snakin-Z and the membrane surface (Figures 4, 5A, and S3), suggesting that CHL likely restricts the peptide interaction mainly to the membrane surface. These findings are in excellent agreement with experimental studies for other antimicrobial peptides and illustrate the role of lipid head groups in the peptide−membrane interactions.[61−63]

The distribution of water molecules around Snakin-Z was significantly affected by its interaction with different membrane models. To quantify this, RDFs were calculated between water molecules and the peptide for all membrane−peptide complexes (Figure 5B). The first peak in each RDF plot (around 0.18−0.22 nm) represents the hydration shell of water molecules close to the peptide. The results revealed distinct hydration patterns. In the BSMP and CAMP membrane models, followed by ECMP, the peak intensity is lower, suggesting a reduced number of water molecules strongly associated with the peptide. This indicates the embedding of Snakin-Z into these membrane models, potentially due to stronger interactions with the lipid bilayer. Conversely, the higher peak in the RBCP RDF implies a more extensive hydration shell around the peptide. This suggests that Snakin-Z interacts less deeply with the RBC membrane model, remaining more exposed to the surrounding water throughout the simulation. Figure 5C depicts the average contact area between Snakin-Z and the various membrane models, which aligns with the findings from the RDF and membrane−peptide distance analyses. The POPG-enriched membrane models, BSMP and CAMP, displayed significantly larger contact areas with the peptide, measuring 9.98 ± 1.83 and 9.09 ± 0.73 nm^2, respectively (Figure 5C). These results suggest stronger interactions between Snakin-Z and the negatively charged POPG-containing membrane models, potentially facilitated by strong electrostatic interactions. In contrast, ECMP and RBCP, containing lower POPG content and CHL (particularly RBCP), displayed a markedly reduced contact area of 8.42 ± 0.78 nm^2 and 6.63 ± 0.34 nm^2, respectively. Statistical analysis revealed that the contact area for RBCP was significantly smaller than for BSMP (p = 0.0066), while no significant differences were observed between RBCP and CAMP (p = 0.0558) or ECMP (p = 0.0831), nor between BSMP, CAMP, and ECMP (all p > 0.05). These results suggest that the peptide interacts more extensively with BSMP membrane models compared to RBCP, while interactions with CAMP and ECMP are intermediate. The presence of CHL in RBCP contributes to a more rigid and tightly packed membrane structure, hindering close peptide−membrane contact and potentially explaining the weaker interaction observed.

To understand how membranes influence the Snakin-Z structure, we investigated the helicity of the peptide across membrane models (Figure S4). The results revealed a remarkably stable α-helical segment encompassing amino acid residues 20−27. This observation aligns well with existing knowledge of antimicrobial peptides like pleurocidin,[34] which adopt and retain α-helices upon interaction with anionic membranes. Notably, in all simulated membrane models, the N-terminal region (residues 20−27) displayed a strong propensity to maintain α-helicity. This is reflected in the

https://doi.org/10.1021/acs.jpcb.5c01013
J. Phys. Chem. B XXXX, XXX, XXX−XXX

consistently high helicity percentages observed in all environments, typically exceeding 75% and often surpassing 90% in BSMP and CAMP. While minor variations in helicity exist, particularly in ECMP, the overall trend suggests preservation of the α-helix across different membrane types.

3.2.3. Peptide–Membrane Interactions. To understand how strongly Snakin-Z binds to membrane models, we computed the average number of contacts and hydrogen bonds (H-bonds) between the peptide and membrane models (Figures 6 and S5). The average number of contacts was

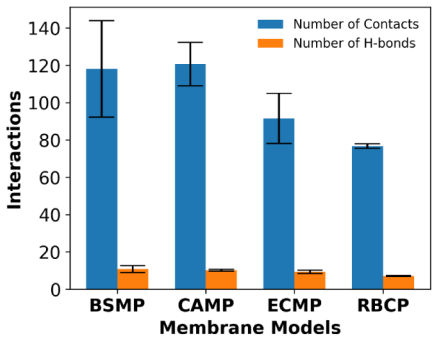

Figure 6. Total number of contacts and H-bonds between Snakin-Z peptide and CAMP, ECMP, and RBCP membranes. Error bars represent the standard error of the mean from triplicate measurements.

highest for CAMP (120.7 ± 11.6) and BSMP (118.1 ± 25.9), followed by ECMP (91.6 ± 13.4) and RBCP (76.7 ± 1.2). A one-way ANOVA revealed significant differences (F = 5.901, p = 0.0200), with RBCP showing significantly fewer contacts than BSMP (p = 0.0224) and CAMP (p = 0.0366). For hydrogen bonds, BSMP (10.8 ± 1.9) and CAMP (10.2 ± 0.5) also showed the highest averages, followed by ECMP (9.3 ± 0.9) and RBCP (7.1 ± 0.3). A one-way ANOVA revealed significant differences in H-bond numbers (F = 9.991, p = 0.0044), with RBCP forming significantly fewer H-bonds than BSMP (p = 0.0034), CAMP (p = 0.0215), and ECMP (p = 0.0319). These results suggest that the peptide forms more extensive contacts and H-bonds with BSMP and CAMP membrane models compared to RBCP, while interactions with ECMP are intermediate. The RDF analysis across membrane–peptide models reveals distinct and lipid-specific interaction patterns between peptide residues (positively charged, polar, and hydrophobic) and various lipid headgroups, highlighting the role of lipids in modulating peptide–membrane interactions (Figures 7 and S6). In the BSMP model, POPG and POPE lipids exhibit strong electrostatic interactions with positively charged residues, with POPG showing a prominent peak at shorter distances compared with POPE, suggesting the dominance of electrostatic forces. Polar and hydrophobic residues interact at longer distances, reflecting weaker hydrogen bonding and hydrophobic effects. Similarly, in the CAMP model, POPG displays a major peak at intermediate distances for all residue types, indicating moderate interactions, while POPI shows exceptionally strong binding with polar residues at close range, driven by hydrogen bonding with the inositol headgroup. POPC exhibits weaker interactions, consistent with their neutral or zwitterionic headgroups. POPE was absent from the immediate vicinity of the peptide. In the ECMP model, POPG demonstrates strong interactions at a close range, reflecting a combination of electrostatic,

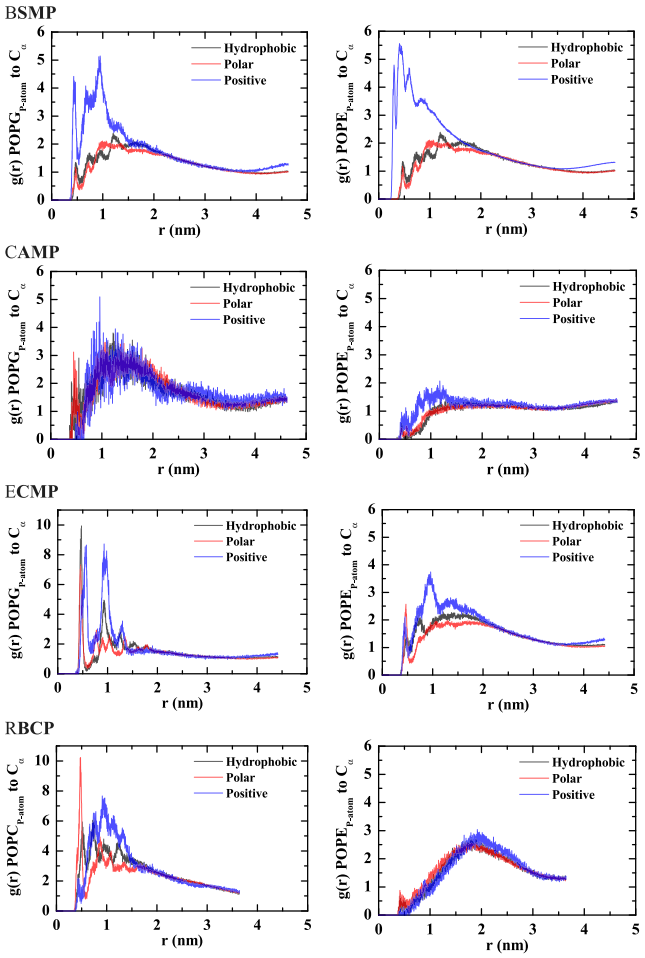

Figure 7. Radial distribution function (RDF) profiles depicting the interactions between phosphorus (P) atoms in the bilayer leaflet, to which the peptide is bound, and the peptide's hydrophobic, polar, and positively charged residues. The RDFs illustrate the spatial distribution of these residue types relative to the lipid headgroups, highlighting variations in interaction strength and localization. Results are shown for one of the replicates, as MD simulations were performed in triplicate.

hydrophobic, and hydrogen bonding forces. POPE, in contrast, shows weaker interactions at close range, with longer-range interactions becoming more significant. In the RBCP model, POPC exhibits strong short-range interactions, with polar residues showing the strongest binding, while POPE shows weak, long-range interactions. Across all models, electrostatic forces dominate interactions with negatively charged lipids (e.g., POPG), while hydrogen bonding and hydrophobic effects play secondary roles. Neutral or zwitterionic lipids (e.g., POPE, POPC) exhibit weaker interactions, with polar residues often showing stronger binding due to hydrogen bonding. These observations underscore the role of lipid headgroup charge and polarity in modulating peptide–membrane interactions. Although PS was included in the symmetric membrane model and appears at the peptide binding site, it is not typically exposed on RBC membranes under physiological conditions.[84]

Additionally, we calculated the contribution of each amino acid to the total number of contacts and H-bonds (Figure 8) to identify crucial residues in membrane–peptide interactions. In the BSMP and CAMP membrane complexes (Figure 8A), N-

https://doi.org/10.1021/acs.jpcb.5c01013
J. Phys. Chem. B XXXX, XXX, XXX–XXX

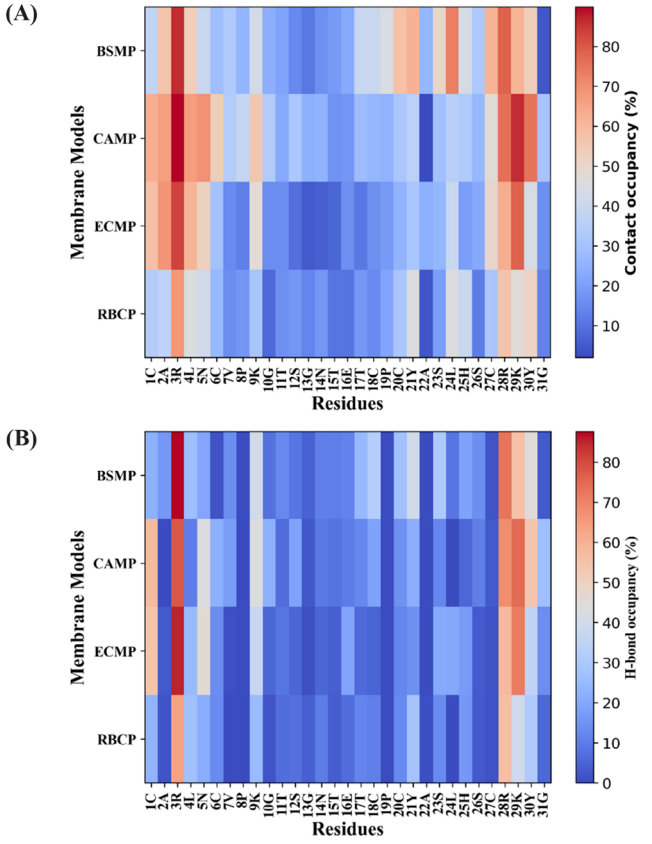

Figure 8. (A) Contact occupancy percentages for Snakin-Z peptide residues with BSMP, CAMP, ECMP, and RBCP membrane models. (B) H-bond occupancy percentages for Snakin-Z peptide residues with these membrane models.

terminal residues (21Y to 30Y) and C-terminal residues (2A to 5N) generally exhibited the highest contact frequencies. Notably, hydrophobic residue Leu4 (4L) and positively charged residues Arg3 (3R), Arg28 (28R), and Lys29 (29K) consistently showed significant contact occupancy across all membrane models. This observation suggests that these specific residues may play a critical role in anchoring the peptide to the membrane surface. The hydrogen bond (H-bond) occupancy data (Figure 8B) provide further insights into the peptide−membrane interactions, complementing the contact occupancy analysis by highlighting the residues most involved in hydrogen bonding. Residues Arg3 (3R), Arg28 (28R), and Lys29 (29K) consistently display high H-bond occupancy across BSMP, CAMP, and ECMP membrane models, emphasizing their crucial role in mediating membrane binding and stabilizing the peptide−membrane complex, as supported by the RDF analysis showing strong electrostatic interactions with anionic lipids. Arg3 shows exceptional H-bond occupancy in BSMP, CAMP, and ECMP, reaching up to 87.7% in BSMP, which emphasizes its importance in anchoring the peptide to the membrane surface. Similarly, Arg28 and Lys29 demonstrate high occupancy with these membrane models, further supporting their role in membrane−peptide complex through electrostatic interactions. Additionally, residues Thr17 (17T) to Cys20 (20C) show notable H-bond occupancy, ranging from 40% to 60%, with the BSMP membrane model but exhibit minimal interaction (15−30%) with other membrane models, suggesting specific binding preferences. Moreover, residues like 30Y exhibit high H-bond occupancy with the CAMP membrane model but lack interactions with the RBCP membrane model, indicating differential binding mechanisms depending on the membrane type.

This variability in contact and H-bond occupancy underscores the intricate nature of peptide−membrane interactions and highlights the importance of specific residue characteristics in dictating binding affinities and functional outcomes within diverse membrane environments. In conclusion, these analyses reveal that the peptide exhibits a higher affinity for the BSMP and CAMP membrane models compared to others, likely due to their lipid composition containing anionic lipid head groups. Specifically, the presence of anionic lipids facilitates strong electrostatic interactions with positively charged residues of the peptide, enhancing its binding affinity. The strong electrostatic interactions between Snakin-Z and anionic lipids are consistent with findings for other antimicrobial peptides (AMPs) , such as pleurocidin, which rely on cationic residues for membrane binding. Pleurocidin exhibits strong binding to anionic membranes, disrupting lipid acyl chain order more effectively in anionic phosphatidylglycerol lipids compared to zwitterionic phosphatidylethanolamine lipids, highlighting the critical role of electrostatic interactions in its activity.[96,97] Similarly, hydrophobic residues play a key role in stabilizing peptide−membrane interactions, as seen in AMPs such as aurein 1.2. Phenylalanine residues in aurein act as membrane anchors, facilitating amphipathic helix positioning at the boundary between lipid headgroups and the hydrophobic core, which stabilizes peptide−membrane interactions and drives membrane disruption through a carpet-like mechanism.[98] These examples underscore the importance of both electrostatic and hydrophobic interactions in mediating AMP activity and membrane binding. Conversely, the peptide exhibits lower affinity for the ECMP and RBCP membrane models due to the absence or lower abundance of anionic lipids in these membrane models.

Further structural analysis revealed selective interactions between Snakin-Z and the membrane models of BSMP, CAMP, ECMP, and RBCP. Figure 9 illustrates these interactions using hydrogen bonds in a representative structure from a highly populated cluster (cluster 1) of Snakin-Z-membrane complexes, as depicted in Figure S2 and Table S1. In the case of BSMP, key hydrogen bonds form between peptide residues (Lys9, Tyr21, Cys18, Cys20, Ser23, and Arg28) and POPG in the membrane. The helical segment of the peptide appears crucial for maintaining these interactions, suggesting a potential mechanism for how Snakin-Z disrupts BSMP. Similarly, for CAMP, hydrogen bonds form between the peptide residues (Cys4, Ser12, Ser13, and Arg28) and membrane lipids, including POPG and POPI. These interactions also align with the RDF results, which highlight the strong binding of polar residues to POPI through hydrogen bonding, further supporting the peptide's embedding mechanism in the membrane. For ECMP, key hydrogen bonds involve residues (Arg28, Lys9, Arg3, and Arg6) and membrane lipids like POPG and POPE. The C- and N-terminal regions seem to play a crucial role, suggesting a mechanism for Snakin-Z to disrupt ECMP. Interestingly, Arg28 is a common interacting residue in BSMP, CAMP, and ECMP. This suggests its critical role in maintaining the stability and function of Snakin-Z across these membrane models, contributing to membrane disruption.

https://doi.org/10.1021/acs.jpcb.5c01013
J. Phys. Chem. B XXXX, XXX, XXX−XXX

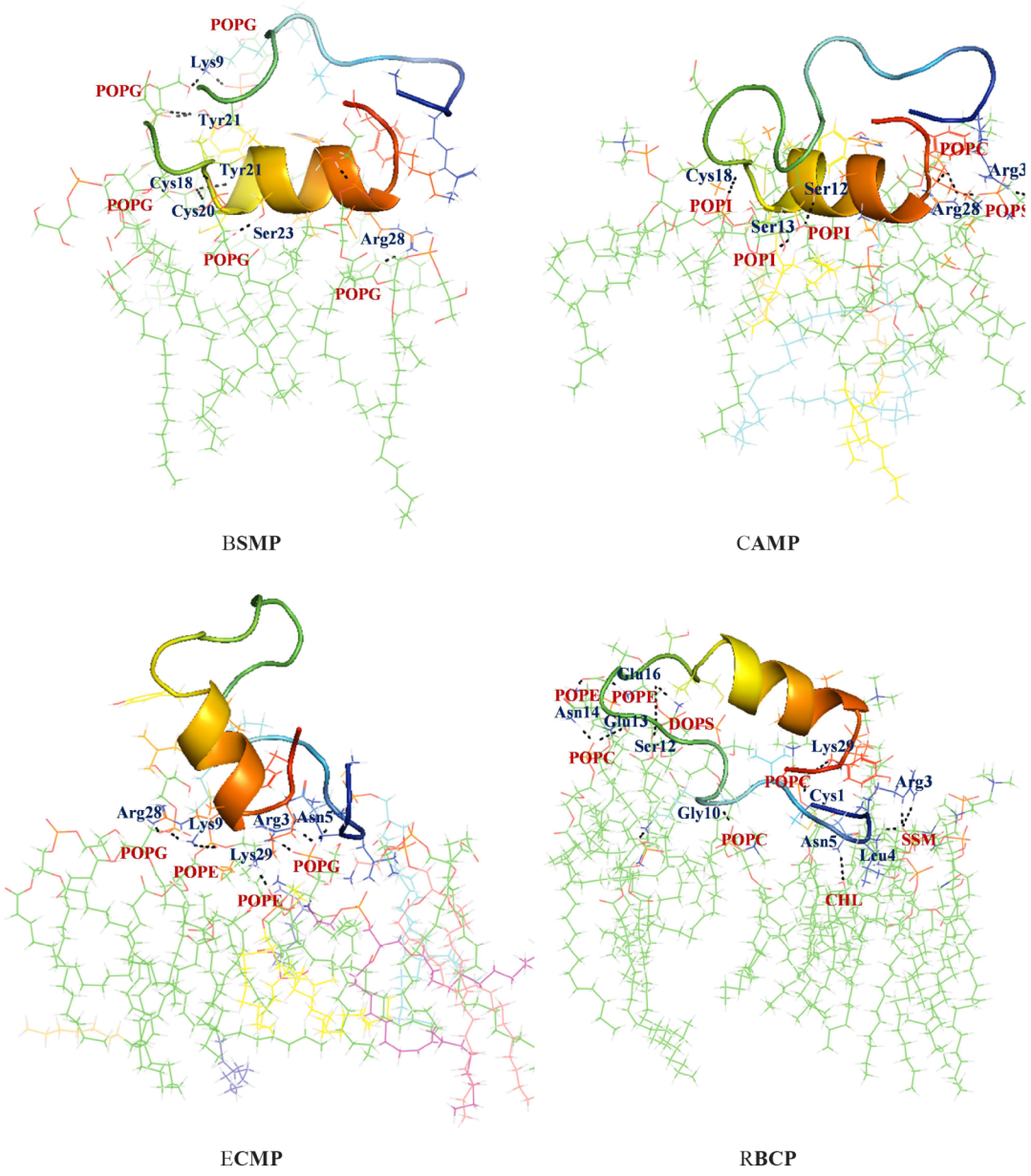

Figure 9. Representative structure of a Snakin-Z and membrane complex, highlighting hydrogen bond interactions along with the residues and lipids involved.

In contrast to the other membrane models, key residues (Lys9, Arg3, Asn5, and Leu14) within RBCP form hydrogen bonds with POPE, POPC, and CHL, establishing a distinct interaction pattern. Notably, this interaction occurs independently of the helical region, suggesting a mechanism by which Snakin-Z interacts with the RBC membrane model without inducing hemolytic activity. This suggests a selective mechanism by which Snakin-Z targets microbial membranes while sparing red blood cells. The simulation results were also supported by the study of Daneshmand et al., who reported that Snakin-Z lacks hemolytic activity.[19] This study, however, for the first time, elucidates how Snakin-Z interacts with membranes. It highlights the importance of the peptide's helical region and specific residues in mediating these crucial interactions with fungal, bacterial, and RBC membrane models. This sheds light on the specificity and potential mechanisms underlying the antimicrobial activity of Snakin-Z, while also explaining its lack of hemolytic activity through its distinct interaction patterns with neutral lipids in RBC membranes. While our simulations show that Snakin-Z retains its helical structure near the lipid headgroups, it is important to note that this observation reflects its behavior under the initial binding conditions. Antimicrobial peptides are known to exhibit significant conformational plasticity, often transitioning from random coil to helical, β-sheet, or β-turn structures as they interact with hydrophobic environments.[89] Such structural transitions may occur over longer time scales or in experimental settings and are critical for understanding the full mechanistic behavior of AMPs. Future studies exploring longer simulation times or experimental validation will provide further insights into these conformational dynamics.

3.3. Structural and Dynamical Changes of Membranes in Response to the Peptide. *3.3.1. Order and Area per Lipid Parameters.* Bacterial membranes are primary

https://doi.org/10.1021/acs.jpcb.5c01013
J. Phys. Chem. B XXXX, XXX, XXX−XXX

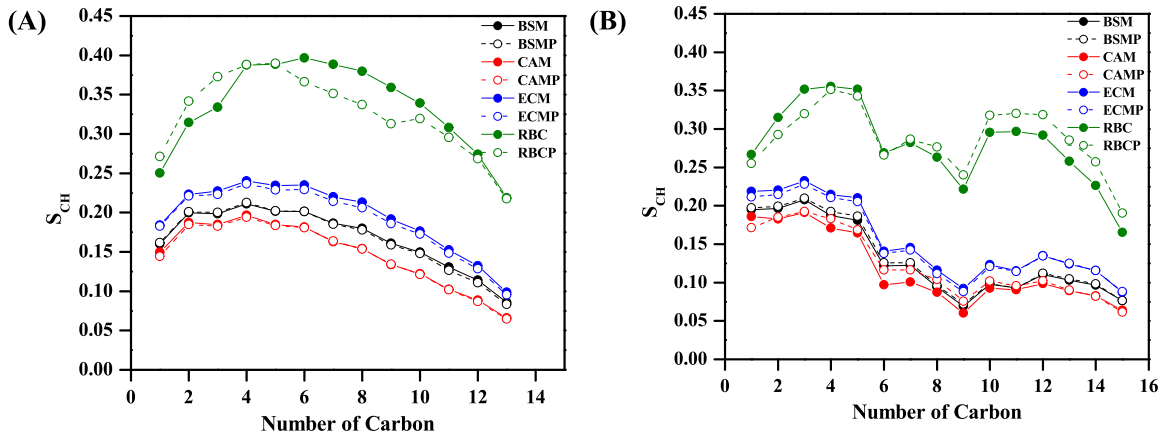

Figure 10. Order parameter of (A) Sn1 and (B) Sn2 acyl chains in the pure bilayer models (BSM, CAM, ECM, and RBC) and their respective peptide−membrane models (BSMP, CAMP, ECMP, and RBCP).

targets for most AMPs.[64] Many studies have investigated how AMPs interact with lipid bilayers, focusing on membrane integrity and peptide structural changes.[60,61,65,66] The composition of lipids in membranes can influence how AMPs function and their overall effectiveness.[67] Notably, the evolution of AMP-resistant bacteria is linked to modifications in lipid composition, which can affect membrane fluidity and integrity.[68,69] AMPs induce a disordering effect on the lipid acyl chains.[62] Consistent with previous computational studies demonstrating that AMPs like melittin, pardaxin, and pleurocidin can disorder lipid acyl chains,[34,70−72] we aimed to understand the mechanisms of action of Snakin-Z by determining how membranes behave dynamically in the presence of this peptide. To understand this, the S_{CH} of the acyl chains was calculated in both pure lipid bilayers and the peptide−membrane complexes, as shown in Figure 10. The S_{CH} of individual lipids obtained from one of the replicas is presented in Figure S7.

Our order parameter results showed that, in all the peptide−membrane systems, the order of acyl chains was decreased by Snakin-Z, except for the RBC membrane model. Interestingly, the order of acyl chains of the RBC membrane model was increased by Snakin-Z, especially in the acyl chain atoms near the headgroup. These results indicated that Snakin-Z can induce further disordering in the anionic phospholipids (Figure S7) relative to the zwitterionic phospholipids, which is in line with experimental results.[73] The S_{CH} values for both acyl chains of ECM and ECMP are higher than those of CAM, CAMP, BSM, and BSMP, which shows that the lipid acyl chain becomes more disordered with increasing levels of anionic lipids. The lipid acyl chains in the RBC membrane model exhibited the highest degree of order among the other membrane models, which is due to the high level of cholesterol in the RBC membrane model. Deuterium NMR investigations have shown that the cholesterol molecules make the lipid acyl chains more ordered.[22] Our previous study clearly elucidated that cholesterol makes the lipid acyl chains more ordered, and specifically, the addition of cholesterol to the phosphatidylcholine membrane increases the lipid chain order.[22] The membranes of these microbes exhibit varying susceptibilities to Snakin-Z, as indicated by their respective minimal inhibitory concentrations (MIC). Notably, *Candida albicans* displayed the lowest MIC value,[19] suggesting heightened sensitivity to Snakin-Z. This finding is consistent with a lower order parameter observed in the case of CAMP, as depicted in Figure 10. The results of the order analysis suggest that Snakin-Z is more sensitive to fungi (CAMP) than bacteria (BAMP and ECMP), which is in accordance with experimental findings.[19,74,75] Paired comparisons between membrane models with and without peptides (e.g., BSM vs BSMP and CAM vs CAMP) showed no significant differences in S_{CH} parameters (all $p > 0.05$). However, a one-way ANOVA revealed significant differences in S_{CH} parameters between membrane models (for sn1: $F = 36.825$, $p < 0.0001$; and for sn2: $F = 32.077$, $p < 0.0001$).

In addition to order parameter analysis, we investigated the influence of Snakin-Z on membrane fluidity by calculating the APL for each system after peptide interaction. Table S2 presents the average APL for triplicate membrane-protein complexes, along with the APL from one replica of the corresponding pure bilayers. APL reflects the average lateral area occupied by a single lipid molecule within the bilayer. Generally, a larger APL indicates a loose and more fluid membrane, whereas a smaller APL suggests a tighter and more rigid environment. The APL values for various lipid species across different membranes revealed interesting trends (Table S2). Notably, POPG consistently exhibited a larger APL compared to POPE in all membrane models containing both lipids (e.g., CAM: POPG = 79.712 ± 10.379 Å² and POPE = 71.548 ± 3.002 Å²). This suggests that POPG, with its negatively charged headgroup, might disfavor tight packing within the membrane, potentially leading to a more fluid environment. This observation is further corroborated by the exceptionally small APL of CHL in the RBCP membrane model (CHL = 29.423 ± 0.988 Å²), indicative of a highly packed and rigid environment compared with other membranes lacking cholesterol. Interestingly, the presence of Snakin-Z has a modest effect on the APL in most membrane models after interaction. The simulated area per lipid (APL) values for the fungal lipid model were compared to experimental data for single-component bilayers (Table S3). While our APL values are larger than those reported experimentally, this discrepancy can be attributed to the heterogeneous composition of the fungal membrane, which includes sterols and sphingolipids that significantly alter lipid packing.[90] Additionally, force field limitations and the simulation time scale may contribute to deviations from experimental values. Despite these differences, the relative trends and behaviors observed in our simulations provide valuable insights into Snakin-Z's interactions with fungal-like

https://doi.org/10.1021/acs.jpcb.5c01013
J. Phys. Chem. B XXXX, XXX, XXX−XXX

membranes, offering a biologically relevant perspective on its mechanism of action.

3.3.2. Membrane Thickness. Membrane thickness was analyzed for both pure lipid bilayers and peptide-bound membrane systems to assess potential structural alterations upon peptide interaction. The temporal evolution of membrane thickness across simulations was analyzed to understand the peptide-induced membrane perturbations (Figure S8). The average membrane thickness was also computed to evaluate localized thinning effects (Figure 11).

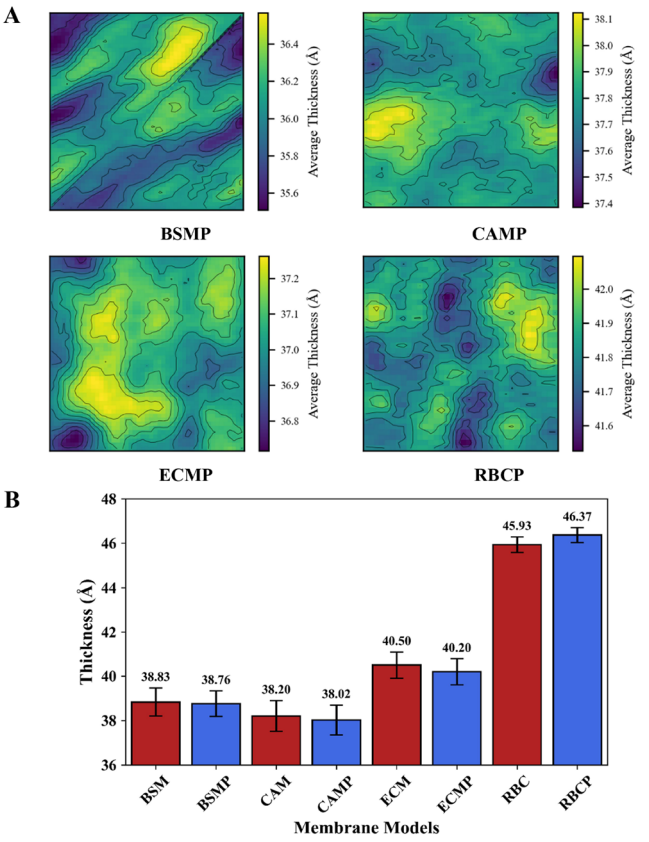

Figure 11. (A) Spatial distribution map of average membrane thickness over last 100 ns. (B) The average membrane thickness in the pure lipid bilayer (red) and the peptide−membrane complex (blue). Error bars represent standard deviations.

Although no significant global disruption was observed, localized perturbations may be evident, as shown in Figure 11A. Figure 10B presents the membrane thickness across different membrane models, comparing peptide-free (BSM, CAM, ECM, and RBC) and peptide-bound (BSMP, CAMP, ECMP, and RBCP) systems. The thickness was highest for RBC (45.93 ± 0.35 Å) and RBCP (46.37 ± 0.34 Å), followed by ECM (40.50 ± 0.60 Å) and ECMP (40.20 ± 0.59 Å), while BSM (38.83 ± 0.63 Å), BSMP (38.76 ± 0.58 Å), CAM (38.20 ± 0.69 Å), and CAMP (38.02 ± 0.67 Å) exhibited the lowest values. A one-way ANOVA revealed a statistically significant difference in membrane thickness among the models (F = 123.058, $p < 0.0001$). Paired comparisons between peptide-free and peptide-bound membranes indicated no significant differences (BSM vs BSMP, p = 1.0; CAM vs CAMP, p = 0.7115; ECM vs ECMP, p = 1.0; and RBC vs RBCP, p = 0.9855), suggesting that Snakin-Z binding does not significantly alter overall membrane thickness. However, localized thinning effects were evident, particularly in CAMP, followed by BSMP and ECMP (Figure 11B). This trend aligns with the observation that Gram-positive membranes, which contain a higher proportion of anionic lipids, exhibited greater thinning compared to Gram-negative membranes. In contrast, cholesterol is primarily found in eukaryotic membranes, such as in RBC and RBCP, known to enhance lipid order and rigidity, likely contributes to their thicker profiles.[22,76] While the overall membrane thickness remained largely unaffected, the deeper penetration of Snakin-Z into the bilayer may induce more pronounced structural alterations, a possibility that warrants further investigation in future studies.

While our 1 μs simulations provide valuable insights into the early-stage interactions of Snakin-Z with lipid membranes, we acknowledge the limitations in capturing full equilibrium dynamics. Longer simulations, such as the 5 μs atomistic MD studies by Tieleman et al.,[88] could reveal more extensive lipid clustering and peptide insertion. Our focus on initial binding events, however, offers a critical perspective on the onset of the antimicrobial activity of Snakin-Z. Future studies will aim to extend simulation time scales and incorporate experimental constraints from techniques like FTIR, neutron reflectometry, or X-ray scattering to refine our models. These approaches could include holding the peptide at experimentally determined locations within the membrane before allowing unrestricted dynamics or employing coarse-grained simulations to access longer time scales. Given the amphiphilic nature of Snakin-Z, we anticipate that extended simulations or experimentally guided models may reveal a deeper penetration into the hydrocarbon or headgroup regions of the membrane. This work lays the foundation for such future investigations, bridging atomistic simulations with experimental observations to enhance our mechanistic understanding of Snakin-Z's membrane interactions.

4. CONCLUSIONS

This study employed all-atom MD simulations to elucidate the molecular basis for the selective binding of Snakin-Z to the prokaryotic *Bacillus subtilis* and *Escherichia coli* membrane models, as well as the eukaryotic *Candida albicans* and RBC membrane models. The results demonstrated that Snakin-Z deeply embedded into the membrane surface of *B. subtilis* and *C. albicans* to a greater extent compared to the *E. coli* and RBC membrane models. This difference can be attributed to the presence of a higher proportion of anionic lipid (POPG, POPS, and POPC) head groups in the membrane models of *B. subtilis* and *C. albicans*. These anionic lipids may electrostatically interact with the cationic residues of Snakin-Z, facilitating stronger binding and deeper penetration. In contrast, the outer membrane of *E. coli* is rich in CLP, which can hinder the interaction of AMPs with the underlying membrane. The RBC membrane model also contains a significant amount of cholesterol, which helps to maintain membrane integrity and reduces the disruptive effects of AMPs. The findings of this study highlight several key determinants for the binding stability and selectivity of Snakin-Z. The amphipathic nature of Snakin-Z's structure, characterized by the presence of both hydrophobic and hydrophilic regions, allows for favorable interactions with the hydrophobic core and polar head groups of membrane lipids. Additionally, the helical region of the peptide plays a crucial role in stabilizing its interaction with the membrane surface. Moreover, the specific lipid composition of the target membrane significantly influences the binding ability

https://doi.org/10.1021/acs.jpcb.5c01013
J. Phys. Chem. B XXXX, XXX, XXX−XXX

of the peptide. Our results suggest that residues such as Arg, Cys, Lys, Ser, and Tyr are directly involved in the binding of Snakin-Z to the membrane models. Notably, Arg 28 was identified as a critical residue for mediating membrane binding and stability of Snakin-Z with *B. subtilis*, *C. albicans*, and *E. coli* membrane models. Membrane-related analyses revealed that Snakin-Z caused local structural thinning and disorder of the acyl chains within the anionic lipid membranes. In contrast, the RBC membrane model exhibited less pronounced structural changes upon interaction with Snakin-Z, further supporting the selectivity of its binding. The findings regarding the influence of cholesterol are particularly noteworthy. Our simulations suggest that cholesterol molecules in the RBC membrane help to maintain their integrity during interactions with Snakin-Z, potentially explaining the extremely low hemolytic activity observed in experiments. This finding suggests that Snakin-Z activity depends on both the lipid head groups and the specific types of hydrophobic acyl chains present in the target membrane bilayer. This knowledge can significantly contribute to the development of next-generation antimicrobials derived from plants. By understanding the mechanisms of action of these natural AMPs, researchers can design more targeted and potent food preservatives with minimal impact on human health. This research paves the way for the development of safer and more effective strategies to combat food spoilage caused by microbial pathogens.

■ ASSOCIATED CONTENT

Data Availability Statement

The data underlying the results presented in this paper are available from Zenodo at https://zenodo.org/records/11644329. This data archive includes all topologies (in.top format), system configurations (in.gro format), parameter files (in.mdp format), output files, and the in-house code used for data processing in this paper. Software used for simulations and analysis is freely available from the following resources: GROMACS (https://manual.gromacs.org/current/download.html), CHARMM-GUI (https://www.charmm-gui.org/?doc=demo&id=qmi&lesson=2), PyMOL (https://pymol.org/), VMD (http://www.ks.uiuc.edu/Research/vmd/), and MDAnalysis (https://www.mdanalysis.org/). More information about the data can be obtained on request from the authors.

Supporting Information

The Supporting Information is available free of charge at https://pubs.acs.org/doi/10.1021/acs.jpcb.5c01013.

Figure S1: modeled structure of Snakin-Z (A) and helical wheel plots (B); Figure S2: representative structures of membrane−peptide complexes; Figure S3: average distance between residue COMs and membrane P atoms; Figure S4: average helicity of Snakin-Z in BSMP, CAMP, ECMP, and RBCP membranes; Figure S5: peptide−membrane interactions: (A) COM contacts and (B) hydrogen bonds; Figure S6: RDF profiles of peptide−lipid interactions. Figure S7: order parameters of Sn1/Sn2 acyl chains and temporal evolution of membrane thickness; Table S1: cluster analysis of membrane−peptide complexes; Table S2: area per lipid (APL) for all membranes; and Table S3: comparison of experimental and simulated APL and membrane thickness for *Candida albicans* membrane (PDF)

■ AUTHOR INFORMATION

Corresponding Author

Yonghui Li − *Department of Grain Science and Industry, Kansas State University, Manhattan, Kansas 66506, United States;* orcid.org/0000-0003-4320-0806; Email: yonghui@ksu.edu

Authors

Nandan Kumar − *Department of Grain Science and Industry, Kansas State University, Manhattan, Kansas 66506, United States;* orcid.org/0000-0001-6915-708X

Zhenjiao Du − *Department of Grain Science and Industry, Kansas State University, Manhattan, Kansas 66506, United States;* orcid.org/0000-0002-8492-4328

Raghavendra G. Amachawadi − *Department of Clinical Sciences, College of Veterinary Medicine, Kansas State University, Manhattan, Kansas 66506, United States*

Xiaolong Guo − *Department of Electrical and Computer Engineering, Kansas State University, Manhattan, Kansas 66506, United States*

Jikai Zhao − *Department of Biological and Agricultural Engineering, Kansas State University, Manhattan, Kansas 66506, United States;* orcid.org/0000-0002-0119-8640

Complete contact information is available at: https://pubs.acs.org/10.1021/acs.jpcb.5c01013

Notes

The authors declare no competing financial interest.

■ ACKNOWLEDGMENTS

This is contribution no. 24-251-J from the Kansas Agricultural Experiment Station.

■ REFERENCES

(1) Hancock, R. E. W.; Sahl, H.-G. Antimicrobial and Host-Defense Peptides as New Anti-Infective Therapeutic Strategies. *Nat. Biotechnol.* **2006**, *24* (12), 1551−1557.

(2) Su, T.; Han, M.; Cao, D.; Xu, M. Molecular and Biological Properties of Snakins: The Foremost Cysteine-Rich Plant Host Defense Peptides. *J. Fungi* **2020**, *6* (4), 220.

(3) Wang, G. The Antimicrobial Peptide Database Provides a Platform for Decoding the Design Principles of Naturally Occurring Antimicrobial Peptides. *Protein Sci.* **2020**, *29* (1), 8−18.

(4) Zhang, Q.-Y.; Yan, Z.-B.; Meng, Y.-M.; Hong, X.-Y.; Shao, G.; Ma, J.-J.; Cheng, X.-R.; Liu, J.; Kang, J.; Fu, C.-Y. Antimicrobial Peptides: Mechanism of Action, Activity and Clinical Potential. *Mil. Med. Res.* **2021**, *8* (1), 48.

(5) Baindara, P.; Mandal, S. M. Plant-Derived Antimicrobial Peptides: Novel Preservatives for the Food Industry. *Foods* **2022**, *11* (16), 2415.

(6) Hintz, T.; Matthews, K. K.; Di, R. The Use of Plant Antimicrobial Compounds for Food Preservation. *Biomed. Res. Int.* **2015**, *2015*, No. e246264.

(7) Sharma, S. Food Preservatives and Their Harmful Effects. *Int. J. Sci. Res. Publ.* **2015**, *5* (4), 1−2.

(8) Shwaiki, L. N.; Arendt, E. K.; Lynch, K. M.; Thery, T. L. C. Inhibitory Effect of Four Novel Synthetic Peptides on Food Spoilage Yeasts. *Int. J. Food Microbiol.* **2019**, *300*, 43−52.

(9) Tam, J. P.; Wang, S.; Wong, K. H.; Tan, W. L. Antimicrobial Peptides from Plants. *Pharmaceuticals* **2015**, *8* (4), 711−757.

(10) Thery, T.; Arendt, E. K. Antifungal Activity of Synthetic Cowpea Defensin Cp-Thionin II and Its Application in Dough. *Food Microbiol.* **2018**, *73*, 111−121.

(11) Zou, F.; Tan, C.; Shinali, T. S.; Zhang, B.; Zhang, L.; Han, Z.; Shang, N. Plant Antimicrobial Peptides: A Comprehensive Review of

Their Classification, Production, Mode of Action, Functions, Applications, and Challenges. *Food Funct.* **2023**, *14* (12), 5492−5515.
(12) Chen, N.; Jiang, C. Antimicrobial Peptides: Structure, Mechanism, and Modification. *Eur. J. Med. Chem.* **2023**, *255*, 115377.
(13) Hof, W. V. T.; Veerman, E. C. I.; Helmerhorst, E. J.; Amerongen, A. V. N.*Antimicrobial Peptides: Properties and Applicability382*De Gruyter2001597−619
(14) Huan, Y.; Kong, Q.; Mou, H.; Yi, H. Antimicrobial Peptides: Classification, Design, Application and Research Progress in Multiple Fields. *Front. Microbiol.* **2020**, *11*, 582779.
(15) López-Solanilla, E.; González-Zorn, B.; Novella, S.; Vázquez-Boland, J. A.; Rodríguez-Palenzuela, P. Susceptibility of Listeria Monocytogenes to Antimicrobial Peptides. *FEMS Microbiol. Lett.* **2003**, *226* (1), 101−105.
(16) Segura, A.; Moreno, M.; Madueño, F.; Molina, A.; García-Olmedo, F. Snakin-1, a Peptide from Potato That Is Active Against Plant Pathogens. *Mol. Plant-Microbe Interact.* **1999**, *12* (1), 16−23.
(17) Shwaiki, L. N.; Arendt, E. K.; Lynch, K. M. Study on the Characterisation and Application of Synthetic Peptide Snakin-1 Derived from Potato Tubers − Action against Food Spoilage Yeast. *Food Control* **2020**, *118*, 107362.
(18) Shwaiki, L. N.; Lynch, K. M.; Arendt, E. K. Future of Antimicrobial Peptides Derived from Plants in Food Application − A Focus on Synthetic Peptides. *Trends Food Sci. Technol.* **2021**, *112*, 312−324.
(19) Daneshmand, F.; Zare-Zardini, H.; Ebrahimi, L. Investigation of the Antimicrobial Activities of Snakin-Z, a New Cationic Peptide Derived from Zizyphus Jujuba Fruits. *Nat. Prod. Res.* **2013**, *27* (24), 2292−2296.
(20) Aronica, P. G. A.; Reid, L. M.; Desai, N.; Li, J.; Fox, S. J.; Yadahalli, S.; Essex, J. W.; Verma, C. S. Computational Methods and Tools in Antimicrobial Peptide Research. *J. Chem. Inf. Model.* **2021**, *61* (7), 3172−3196.
(21) Bogdanova, L. R.; Valiullina, Y. A.; Faizullin, D. A.; Kurbanov, R. K.; Ermakova, E. A. Spectroscopic, Zeta Potential and Molecular Dynamics Studies of the Interaction of Antimicrobial Peptides with Model Bacterial Membrane. *Spectrochim. Acta, Part A* **2020**, *242*, 118785.
(22) Kumar, N.; Sastry, G. N. Study of Lipid Heterogeneity on Bilayer Membranes Using Molecular Dynamics Simulations. *J. Mol. Graphics Modell.* **2021**, *108*, 108000.
(23) Matamoros-Recio, A.; Franco-Gonzalez, J. F.; Forgione, R. E.; Torres-Mozas, A.; Silipo, A.; Martín-Santamaría, S. Understanding the Antibacterial Resistance: Computational Explorations in Bacterial Membranes. *ACS Omega* **2021**, *6* (9), 6041−6054.
(24) Sharma, P.; Parthasarathi, S.; Patil, N.; Waskar, M.; Raut, J. S.; Puranik, M.; Ayappa, K. G.; Basu, J. K. Assessing Barriers for Antimicrobial Penetration in Complex Asymmetric Bacterial Membranes: A Case Study with Thymol. *Langmuir* **2020**, *36* (30), 8800−8814.
(25) Vaiwala, R.; Sharma, P.; Ganapathy Ayappa, K. Differentiating Interactions of Antimicrobials with Gram-Negative and Gram-Positive Bacterial Cell Walls Using Molecular Dynamics Simulations. *Biointerphases* **2022**, *17* (6), 061008.
(26) Wang, K.; Shao, X.; Cai, W. Binding Models of Aβ42 Peptide with Membranes Explored by Molecular Simulations. *J. Chem. Inf. Model.* **2022**, *62* (24), 6482−6493.
(27) Kumar, N.; Rani, P.; Agarwal, S.; Singh, D. V. 6-Ethoxy-4- N-(2-Morpholin-4-Ylethyl) −2-N-Propan-2-Yl-1,3, 5-Triazine-2, 4-Diamine Endows Herbicidal Activity against Phalaris Minor a Weed of Wheat Crop Field: An in -Silico and Experimental Approaches of Herbicide Discovery. *J. Mol. Model.* **2022**, *28* (4), 77.
(28) Kumar, N.; Gaur, A. S.; Sastry, G. N. A Perspective on the Nature of Cation-π Interactions. *J. Chem. Sci.* **2021**, *133* (4), 97.
(29) Kumar, N.; Saha, S.; Sastry, G. N. Towards Developing a Criterion to Characterize Non-Covalent Bonds: A Quantum Mechanical Study. *Phys. Chem. Chem. Phys.* **2021**, *23* (14), 8478−8488.
(30) Bhargav Kumar, Y.; Kumar, N.; John, L.; Mahanta, H. J.; Vaikundamani, S.; Nagamani, S.; Madhavi Sastry, G.; Narahari Sastry, G. Analyzing the Cation-aromatic Interactions in Proteins: Cation-aromatic Database V2.0. *Proteins* **2023**, *92*, 179−191.
(31) Kumar, Y. B.; Kumar, N.; Vaikundamani, S.; Nagamani, S.; Mahanta, H. J.; Sastry, G. M.; Sastry, G. N. Analyzing the Aromatic-Aromatic Interactions in Proteins: A2ID 2.0. *Int. J. Biol. Macromol.* **2023**, *253*, 127207.
(32) Sohlenkamp, C.; Geiger, O. Bacterial Membrane Lipids: Diversity in Structures and Pathways. *FEMS Microbiol. Rev.* **2016**, *40* (1), 133−159.
(33) Bernat, P.; Paraszkiewicz, K.; Siewiera, P.; Moryl, M.; Płaza, G.; Chojniak, J. Lipid Composition in a Strain of Bacillus Subtilis, a Producer of Iturin A Lipopeptides That Are Active against Uropathogenic Bacteria. *World J. Microbiol. Biotechnol.* **2016**, *32* (10), 157.
(34) Talandashti, R.; Mahdiuni, H.; Jafari, M.; Mehrnejad, F. Molecular Basis for Membrane Selectivity of Antimicrobial Peptide Pleurocidin in the Presence of Different Eukaryotic and Prokaryotic Model Membranes. *J. Chem. Inf. Model.* **2019**, *59* (7), 3262−3276.
(35) Hitchcock, C. A.; Barrett-Bee, K. J.; Russell, N. J. The Lipid Composition of y and Azole-Resistant Strains of Candida Albicans. *Microbiology* **1986**, *132* (9), 2421−2431.
(36) Wang, G.; Li, X.; Wang, Z. APD3: The Antimicrobial Peptide Database as a Tool for Research and Education. *Nucleic Acids Res.* **2016**, *44* (D1), D1087−D1093.
(37) Yang, J.; Zhang, Y. I-TASSER Server: New Development for Protein Structure and Function Predictions. *Nucleic Acids Res.* **2015**, *43* (W1), W174−W181.
(38) Wu, E. L.; Cheng, X.; Jo, S.; Rui, H.; Song, K. C.; Dávila-Contreras, E. M.; Qi, Y.; Lee, J.; Monje-Galvan, V.; Venable, R. M. CHARMM-GUI Membrane Builder toward Realistic Biological Membrane Simulations. *J. Comput. Chem.* **2014**, *35* (27), 1997−2004.
(39) Jafari, M.; Mehrnejad, F.; Aghdami, R.; Chaparzadeh, N.; Razaghi Moghadam Kashani, Z.; Doustdar, F. Identification of the Crucial Residues in the Early Insertion of Pardaxin into Different Phospholipid Bilayers. *J. Chem. Inf. Model.* **2017**, *57* (4), 929−941.
(40) Venable, R. M.; Krämer, A.; Pastor, R. W. Molecular Dynamics Simulations of Membrane Permeability. *Chem. Rev.* **2019**, *119* (9), 5954−5997.
(41) Xiang, N.; Lyu, Y.; Zhu, X.; Narsimhan, G. Investigation of the Interaction of Amyloid β Peptide (11−42) Oligomers with a 1-Palmitoyl-2-Oleoyl-Sn-Glycero-3-Phosphocholine (POPC) Membrane Using Molecular Dynamics Simulation. *Phys. Chem. Chem. Phys.* **2018**, *20* (10), 6817−6829.
(42) Abraham, M. J.; Murtola, T.; Schulz, R.; Páll, S.; Smith, J. C.; Hess, B.; Lindahl, E. GROMACS: High Performance Molecular Simulations through Multi-Level Parallelism from Laptops to Supercomputers. *SoftwareX* **2015**, *1*, 19−25.
(43) Best, R. B.; Zhu, X.; Shim, J.; Lopes, P. E. M.; Mittal, J.; Feig, M.; MacKerell, A. D., Jr. Optimization of the Additive CHARMM All-Atom Protein Force Field Targeting Improved Sampling of the Backbone ϕ, ψ and Side-Chain X1 and X2 Dihedral Angles. *J. Chem. Theory Comput.* **2012**, *8* (9), 3257−3273.
(44) Klauda, J. B.; Venable, R. M.; Freites, J. A.; O'Connor, J. W.; Tobias, D. J.; Mondragon-Ramirez, C.; Vorobyov, I.; MacKerell, A. D., Jr.; Pastor, R. W. Update of the CHARMM All-Atom Additive Force Field for Lipids: Validation on Six Lipid Types. *J. Phys. Chem. B* **2010**, *114* (23), 7830−7843.
(45) Essex, J. W.; Hann, M. M.; Graham Richards, W. Molecular Dynamics Simulation of a Hydrated Phospholipid Bilayer. *Philos. Trans. R. Soc. London, Ser. B* **1994**, *344* (1309), 239−260.
(46) Jo, S.; Kim, T.; Iyer, V. G.; Im, W. CHARMM-GUI: A Web-Based Graphical User Interface for CHARMM. *J. Comput. Chem.* **2008**, *29* (11), 1859−1865.
(47) van Meer, G.; Voelker, D. R.; Feigenson, G. W. Membrane Lipids: Where They Are and How They Behave. *Nat. Rev. Mol. Cell Biol.* **2008**, *9* (2), 112−124.

https://doi.org/10.1021/acs.jpcb.5c01013
J. Phys. Chem. B XXXX, XXX, XXX−XXX

(48) Hoover, W. G. Canonical Dynamics: Equilibrium Phase-Space Distributions. *Phys. Rev. A* **1985**, *31* (3), 1695−1697.
(49) Nosé, S. A Molecular Dynamics Method for Simulations in the Canonical Ensemble. *Mol. Phys.* **1984**, *52* (2), 255−268.
(50) Parrinello, M.; Rahman, A. Polymorphic Transitions in Single Crystals: A New Molecular Dynamics Method. *J. Appl. Phys.* **1981**, *52* (12), 7182−7190.
(51) Hess, B. P-LINCS: A Parallel Linear Constraint Solver for Molecular Simulation. *J. Chem. Theory Comput.* **2008**, *4* (1), 116−122.
(52) Darden, T.; York, D.; Pedersen, L. Particle Mesh Ewald: An $N \cdot \log(N)$ Method for Ewald Sums in Large Systems. *J. Chem. Phys.* **1993**, *98* (12), 10089−10092.
(53) Essmann, U.; Perera, L.; Berkowitz, M. L.; Darden, T.; Lee, H.; Pedersen, L. G. A Smooth Particle Mesh Ewald Method. *J. Chem. Phys.* **1995**, *103* (19), 8577−8593.
(54) Humphrey, W.; Dalke, A.; Schulten, K. VMD: Visual Molecular Dynamics. *J. Mol. Graphics* **1996**, *14* (1), 33−38.
(55) Gowers, R. J.; Linke, M.; Barnoud, J.; Reddy, T. J. E.; Melo, M. N.; Seyler, S. L.; Domański, J.; Dotson, D. L.; Buchoux, S.; Kenney, I. M.et al.MDAnalysis: A Python Package for the Rapid Analysis of Molecular Dynamics Simulations*Proceedings of the 15th Python in Science Conference*SCIPY201698−105
(56) Guixà-González, R.; Rodriguez-Espigares, I.; Ramírez-Anguita, J. M.; Carrió-Gaspar, P.; Martinez-Seara, H.; Giorgino, T.; Selent, J. MEMBPLUGIN: Studying Membrane Complexity in VMD. *Bioinformatics* **2014**, *30* (10), 1478−1480.
(57) Ghanbarzadeh, Z.; Hemmati, S.; Mohagheghzadeh, A. Humanizing Plant-Derived Snakins and Their Encrypted Antimicrobial Peptides. *Biochimie* **2022**, *199*, 92−111.
(58) Teker, T.; Albayrak, G.; Turan, K. Heterologous Expression and Initial In Silico Characterization of a Novel Snakin-Z Peptide. *Int. J. Pept. Res. Ther.* **2023**, *29* (5), 84.
(59) Erdem Büyükkiraz, M.; Kesmen, Z. Antimicrobial Peptides (AMPs): A Promising Class of Antimicrobial Compounds. *J. Appl. Microbiol.* **2022**, *132* (3), 1573−1596.
(60) Mason, A. J.; Marquette, A.; Bechinger, B. Zwitterionic Phospholipids and Sterols Modulate Antimicrobial Peptide-Induced Membrane Destabilization. *Biophys. J.* **2007**, *93* (12), 4289−4299.
(61) Lan, Y.; Ye, Y.; Kozlowska, J.; Lam, J. K. W.; Drake, A. F.; Mason, A. J. Structural Contributions to the Intracellular Targeting Strategies of Antimicrobial Peptides. *Biochim. Biophys. Acta, Biomembr.* **2010**, *1798* (10), 1934−1943.
(62) Mason, A. J.; Chotimah, I. N. H.; Bertani, P.; Bechinger, B. A Spectroscopic Study of the Membrane Interaction of the Antimicrobial Peptide Pleurocidin. *Mol. Membr. Biol.* **2006**, *23* (2), 185−194.
(63) Yoshida, K.; Mukai, Y.; Niidome, T.; Takashi, C.; Tokunaga, Y.; Hatakeyama, T.; Aoyagi, H. Interaction of Pleurocidin and Its Analogs with Phospholipid Membrane and Their Antibacterial Activity. *J. Pept. Res.* **2001**, *57* (2), 119−126.
(64) Sato, H.; Feix, J. B. Peptide−Membrane Interactions and Mechanisms of Membrane Destruction by Amphipathic α-Helical Antimicrobial Peptides. *Biochim. Biophys. Acta, Biomembr.* **2006**, *1758* (9), 1245−1256.
(65) Galdiero, S.; Falanga, A.; Cantisani, M.; Vitiello, M.; Morelli, G.; Galdiero, M. Peptide-Lipid Interactions: Experiments and Applications. *Int. J. Mol. Sci.* **2013**, *14* (9), 18758−18789.
(66) Urbina, J. A.; Pekerar, S.; Le, H.; Patterson, J.; Montez, B.; Oldfield, E. Molecular Order and Dynamics of Phosphatidylcholine Bilayer Membranes in the Presence of Cholesterol, Ergosterol and Lanosterol: A Comparative Study Using 2H-, 13C- and 31P-NMR Spectroscopy. *Biochim. Biophys. Acta, Biomembr.* **1995**, *1238* (2), 163−176.
(67) Lee, T.-H.; Sani, M.-A.; Overall, S.; Separovic, F.; Aguilar, M.-I. Effect of Phosphatidylcholine Bilayer Thickness and Molecular Order on the Binding of the Antimicrobial Peptide Maculatin 1.1. *Biochim. Biophys. Acta, Biomembr.* **2018**, *1860* (2), 300−309.
(68) Mishra, N. N.; Bayer, A. S. Correlation of Cell Membrane Lipid Profiles with Daptomycin Resistance in Methicillin-Resistant Staphylococcus Aureus. *Antimicrob. Agents Chemother.* **2013**, *57* (2), 1082−1085.
(69) Omardien, S.; Brul, S.; Zaat, S. A. J. Antimicrobial Activity of Cationic Antimicrobial Peptides against Gram-Positives: Current Progress Made in Understanding the Mode of Action and the Response of Bacteria. *Front. Cell Dev. Biol.* **2016**, *4*, 111.
(70) Jafari, M.; Mehrnejad, F.; Doustdar, F. Insight into the Interactions, Residue Snorkeling, and Membrane Disordering Potency of a Single Antimicrobial Peptide into Different Lipid Bilayers. *PLoS One* **2017**, *12* (11), No. e0187216.
(71) Sengupta, D.; Leontiadou, H.; Mark, A. E.; Marrink, S.-J. Toroidal Pores Formed by Antimicrobial Peptides Show Significant Disorder. *Biochim. Biophys. Acta, Biomembr.* **2008**, *1778* (10), 2308−2317.
(72) Zhao, L.; Cao, Z.; Bian, Y.; Hu, G.; Wang, J.; Zhou, Y. Molecular Dynamics Simulations of Human Antimicrobial Peptide LL-37 in Model POPC and POPG Lipid Bilayers. *Int. J. Mol. Sci.* **2018**, *19* (4), 1186.
(73) Amos, S.-B. T. A.; Vermeer, L. S.; Ferguson, P. M.; Kozlowska, J.; Davy, M.; Bui, T. T.; Drake, A. F.; Lorenz, C. D.; Mason, A. J. Antimicrobial Peptide Potency Is Facilitated by Greater Conformational Flexibility When Binding to Gram-Negative Bacterial Inner Membranes. *Sci. Rep.* **2016**, *6* (1), 37639.
(74) Manners, J. M. Primitive Defence: The MiAMP1 Antimicrobial Peptide Family. *Plant Mol. Biol. Rep.* **2009**, *27* (3), 237−242.
(75) Selitrennikoff, C. P. Antifungal Proteins. *Appl. Environ. Microbiol.* **2001**, *67* (7), 2883−2894.
(76) de Meyer, F.; Smit, B. Effect of Cholesterol on the Structure of a Phospholipid Bilayer. *Proc. Natl. Acad. Sci. U. S. A.* **2009**, *106* (10), 3654−3658.
(77) Kumar, N.; Du, Z.; Li, Y. pLM4CPPs: Protein Language Model-Based Predictor for Cell Penetrating Peptides. *J. Chem. Inf. Model.* **2025**, *65* (3), 1128−1139.
(78) Du, Z.; Ding, X.; Xu, Y.; Li, Y. UniDL4BioPep: A universal deep learning architecture for binary classification in peptide bioactivity. *Briefings Bioinf.* **2023**, *24*, bbad135.
(79) Heinig, M.; Frishman, D. STRIDE: A web server for secondary structure assignment from known atomic coordinates of proteins. *Nucleic Acids Res.* **2004**, *32*, W500−W502.
(80) Michaud-Agrawal, N.; Denning, E. J.; Woolf, T. B.; Beckstein, O. MDAnalysis: A Toolkit for the Analysis of Molecular Dynamics Simulations. *J. Comput. Chem.* **2011**, *32*, 2319−2327.
(81) Prasad, R.; Singh, A. Lipids of Candida albicans and Their Role in Multidrug Resistance. *Curr. Genet.* **2013**, *59* (4), 243−250.
(82) Loh, R. K.; Huestis, W. H. Human Erythrocyte Membrane Lipid Asymmetry: Transbilayer Distribution of Rapidly Diffusing Phosphatidylserines. *Biochemistry* **1993**, *32* (43), 11722−11726.
(83) Pavan, C.; Sydor, M. J.; Bellomo, C.; Leinardi, R.; Cananà, S.; Kendall, R. L.; Rebba, E.; Corno, M.; Ugliengo, P.; Mino, L.; Holian, A.; Turci, F. Molecular recognition between membrane epitopes and nearly free surface silanols explains silica membranolytic activity. *Colloids Surf., B* **2022**, *217*, 112625.
(84) Lorent, J. H.; Levental, K. R.; Ganesan, L.; Rivera-Longsworth, G.; Sezgin, E.; Doktorova, M.; Levental, I. Plasma Membranes Are Asymmetric in Lipid Unsaturation, Packing and Protein Shape. *Nat. Chem. Biol.* **2020**, *16* (6), 644−652.
(85) Lattif, A. A.; Mukherjee, P. K.; Chandra, J.; Roth, M. R.; Welti, R.; Rouabhia, M.; Ghannoum, M. A. Lipidomics of Candida albicans Biofilms Reveals Phase-Dependent Production of Phospholipid Molecular Classes and Role for Lipid Rafts in Biofilm Formation. *Microbiology* **2011**, *157* (11), 3232−3242.
(86) Mishra, N. N.; Prasad, T.; Sharma, N.; Gupta, D. K. Membrane Fluidity and Lipid Composition of Fluconazole Resistant and Susceptible Strains of Candida albicans Isolated from Diabetic Patients. *Braz. J. Microbiol.* **2008**, *39*, 219−225.
(87) Ghannoum, M. A.; Janini, G.; Khamis, L.; Radwan, S. S. Dimorphism-Associated Variations in the Lipid Composition of Candida albicans. *Microbiology* **1986**, *132* (8), 2367−2375.

https://doi.org/10.1021/acs.jpcb.5c01013
J. Phys. Chem. B XXXX, XXX, XXX−XXX

(88) Gu, R. X.; Baoukina, S.; Tieleman, D. P. Phase Separation in Atomistic Simulations of Model Membranes. *J. Am. Chem. Soc.* **2020**, *142* (6), 2844−2856.
(89) Andrew Woolley, A.; Wallace, B. A. Model Ion Channels: Gramicidin and Alamethicin. *J. Membr. Biol.* **1992**, *129* (2), 109−136.
(90) Ingólfsson, H. I.; Arnarez, C.; Periole, X.; Marrink, S. J. Computational 'Microscopy' of Cellular Membranes. *J. Cell Sci.* **2016**, *129* (2), 257−268.
(91) Agrawal, P.; Bhalla, S.; Chaudhary, K.; Kumar, R.; Sharma, M.; Raghava, G. P. S. In Silico Approach for Prediction of Antifungal Peptides. *Front. Microbiol.* **2018**, *9*, 323.
(92) Zhu, X.; Zhang, L.; Wang, J.; Ma, Z.; Xu, W.; Li, J.; Shan, A. Characterization of Antimicrobial Activity and Mechanisms of Low Amphipathic Peptides with Different α-Helical Propensity. *Acta Biomater.* **2015**, *18*, 155−167.
(93) Manzo, G.; Ferguson, P. M.; Hind, C. K.; Clifford, M.; Gustilo, V. B.; Ali, H.; Bansal, S. S.; Bui, T. T.; Drake, A. F.; Atkinson, R. A.; Sutton, J. M.; Lorenz, C. D.; Phoenix, D. A.; Mason, A. J. Temporin L and Aurein 2.5 Have Identical Conformations but Subtly Distinct Membrane and Antibacterial Activities. *Sci. Rep.* **2019**, *9* (1), 10934.
(94) Manzo, G.; Ferguson, P. M.; Gustilo, V. B.; Hind, C. K.; Clifford, M.; Bui, T. T.; Drake, A. F.; Atkinson, R. A.; Sutton, J. M.; Batoni, G.; Lorenz, C. D.; Phoenix, D. A.; Mason, A. J. Minor Sequence Modifications in Temporin B Cause Drastic Changes in Antibacterial Potency and Selectivity by Fundamentally Altering Membrane Activity. *Sci. Rep.* **2019**, *9* (1), 1385.
(95) Shahmiri, M.; Enciso, M.; Adda, C. G.; Smith, B. J.; Perugini, M. A.; Mechler, A. Membrane Core-Specific Antimicrobial Action of Cathelicidin LL-37 Peptide Switches Between Pore and Nanofibre Formation. *Sci. Rep.* **2016**, *6*, 38184.
(96) Mason, A. J.; Chotimah, I. N.; Bertani, P.; Bechinger, B. A Spectroscopic Study of the Membrane Interaction of the Antimicrobial Peptide Pleurocidin. *Mol. Membr. Biol.* **2006**, *23* (2), 185−194.
(97) (a) Amos, S. T. A.; Vermeer, L. S.; Ferguson, P. M.; Kozlowska, J.; Davy, M.; Bui, T. T.; Drake, A. F.; Lorenz, C. D.; James Mason, A. Author Correction: Antimicrobial Peptide Potency is Facilitated by Greater Conformational Flexibility when Binding to Gram-negative Bacterial Inner Membranes. *Sci. Rep.* **2018**, *8* (1), 17073. (b) Amos, S. B. T.; Vermeer, L. S.; Ferguson, P. M.; Kozlowska, J.; Davy, M.; Bui, T. T.; Drake, A. F.; Lorenz, C. D.; James Mason, A. Antimicrobial Peptide Potency is Facilitated by Greater Conformational Flexibility when Binding to Gram-negative Bacterial Inner Membranes. *Sci. Rep.* **2016**, *6*, 37639.
(98) Shahmiri, M.; Enciso, M.; Mechler, A. Controls and Constrains of the Membrane Disrupting Action of Aurein 1.2. *Sci. Rep.* **2015**, *5*, 16378.

https://doi.org/10.1021/acs.jpcb.5c01013
J. Phys. Chem. B XXXX, XXX, XXX−XXX